Taylor & Francis
Taylor & Francis Group

RESEARCH PAPER

OPEN ACCESS | Check for updates

Discovery of new symmetrical and asymmetrical nitrile-containing 1,4-dihydropyridine derivatives as dual kinases and P-glycoprotein inhibitors: synthesis, *in vitro* assays, and *in silico* studies

Mohamed H. Saad[a], Tarek F. El-Moselhy[b], Nabaweya S, El-Din[b], Ahmed B. M. Mehany[c] (iD), Amany Belal[d,e] (iD), Mohammed A. S. Abourehab[f,g] (iD), Haytham O. Tawfik[b] (iD) and Mervat H. El-Hamamsy[b]

[a]The Egyptian Ministry of Health, Tanta, Egypt; [b]Department of Pharmaceutical Chemistry, Faculty of Pharmacy, Tanta University, Tanta, Egypt; [c]Zoology Department, Faculty of Science, Al-Azhar University, Cairo, Egypt; [d]Medicinal Chemistry Department, Faculty of Pharmacy, Beni-Suef University, Beni-Suef, Egypt; [e]Department of Pharmaceutical Chemistry, College of Pharmacy, Taif University, Taif, Saudi Arabia; [f]Department of Pharmaceutics, Faculty of Pharmacy, Umm Al-Qura University, Makkah, Saudi Arabia; [g]Department of Pharmaceutics and Industrial Pharmacy, College of Pharmacy, Minia University, Minia, Egypt

ABSTRACT

Two new series of symmetric (**1a-h**) and asymmetric (**2a-l**) 1,4-DHP derivatives were designed, synthesised, and evaluated as anticancer agents. *In vitro* anticancer screening of target compounds *via* National cancer institute "NCI" revealed that analogues **1g**, **2e**, and **2l** demonstrated antiproliferative action with mean growth inhibition percentage "GI%" = 41, 28, and 64, respectively. The reversal doxorubicin (DOX) effects of compounds **1g**, **2e**, and **2l** were examined and illustrated better cytotoxic activity with IC_{50} =1.12, 3.64, and 3.57 μM, respectively. The most active anticancer analogues, **1g**, **2e**, and **2l**, were inspected for their putative mechanism of action by estimating their epidermal growth factor receptor (EGFR), human epidermal growth factor receptor 2 (HER-2), and Bruton's tyrosine kinase (BTK) inhibitory activities. Furthermore, the antimicrobial activity of target compounds was assessed against six different pathogens, followed by determining the minimum inhibitory concentration "MIC" values for the most active analogues. Molecular docking study was achieved to understand mode of interactions between selected inhibitors and different biological targets.

1. Introduction

Cancer is still the second leading cause of death worldwide, despite advances in its treatment and prevention. However, the effectiveness of cancer treatment in the twenty-first century is still a worry, and new and safer anticancer drugs with a broader range of cytotoxicity to tumour cells need to be researched.[1,2] Many types of cancers arise as a result of the ability of cells to proliferate indefinitely and their inherent resistance to apoptosis. Tumour cells have the potential to stimulate their self-proliferation *via* biological pathways, including meiotic cell division, which contributes to carcinogenesis.[3,4] Relying on new evidence, kinases proteins such as receptor tyrosine kinases (RTKs) and cyclin-dependent kinases (CDKs) are the most extensively studied targets in diverse carcinogenic signalling pathways because they have been involved in highly conserved physiological processes such as cell proliferation, mitosis, and cell division.[5,6] Aberrant or excessive production of these proteins disrupts the normal regulation of the cell cycle, which is seen in a variety of cancers. Accordingly, kinases inhibitors interfere directly with biological processes, preventing excessive cell proliferation and tumour progression.[7,8] It was found that 1,4-dihydropyridines (1,4-DHPs) could be promising RTK and CDK inhibitors.[9–11]

There are many 1,4-DHPs with variable structures that showed anticancer activity in many cancer cell lines, where they could disrupt the survival of tumour cells by different mechanisms.[12] Compound **I** having 1,4-DHP ring, displayed apoptotic effect in human melanoma; A375 cell line, and human liver cancer; HepG2 cell line through its capability of binding to the allosteric site of SIRT1, resulting in its activation[13,14] as illustrated in Figure 1. Whereas activation of NAD^+-dependent deacetylase SIRT1 inhibits tumorigenesis by promoting apoptosis by suppressing the transcription factor NF-κB. Compound **II** demonstrated good RTK inhibitory activity, exhibiting IC_{50}=68.80, 71.79, and 84.51 nM against Bruton's tyrosine kinase (BTK), epidermal growth factor receptor (EGFR), and human epidermal growth factor receptor 2 (HER-2), respectively, compared to erlotinib, IC_{50} = 59.41, 49.13, and 74.73 nM respectively,[15] as shown in Figure 1.

Unfortunately, multidrug resistance (MDR) in cancer is a pleiotropic complex phenomenon by which some drug-resistant tumour cells gain the ability to overcome the effect of unrelated chemotherapeutic agents regardless of their chemical structure and mechanism of action. So, MDR is considered the major obstacle in cancer treatment nowadays. Many mechanisms are involved in cancer MDR;[16,17] the most important one is ATP
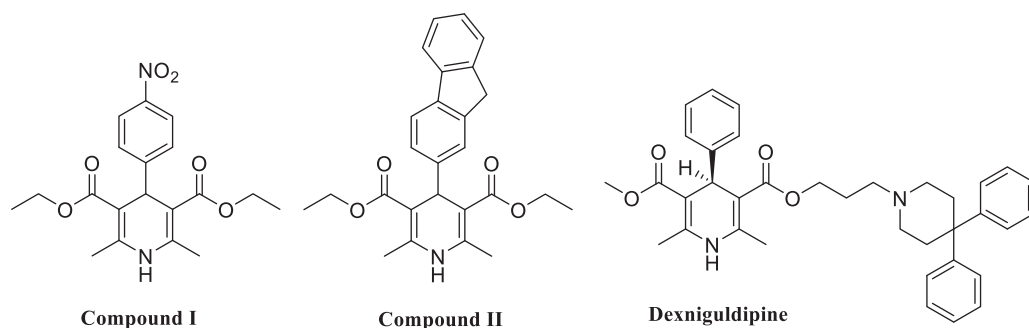

Figure 1. Structure of some reported biologically active 1,4-DHP derivatives.

binding cassette (ABC) protein transporters, specially permeation protein (P-glycoprotein [P-gp]).[18,19]

1,4-DHPs such as dexniguldipine (Figure 1) was one of the potent P-gp inhibitors lacking calcium antagonistic activity.[20,21] Dexniguldipine is the (−)-enantiomer of the asymmetric 1,4-DHP, niguldipine, that is 40 times less potent than (+)-niguldipine in its interaction with L-type calcium channels. Hence, structural modifications on the 1,4-DHP scaffold were performed to generate 1,4-DHP derivatives having better P-gp inhibitory activity and less calcium antagonistic activity. A series of 1,4-DHP niguldipine analogues were synthesised, and their effects on daunomycin cytotoxicity against HCT-116/ADR (a resistant variant of the human breast cancer HCT-116 cell line over expresses P-gp) were investigated.[22] It was reported that 1,4-DHPs compounds lacking or having low calcium channel antagonistic activity retained MDR reversal property, which was dependent on the nature of the substituent at 3- and 5- positions of the DHP ring. Ester groups at 3- and 5- positions of the DHP ring were essential for calcium channel antagonistic activity, thus, replacement of these groups could reduce cardiovascular side effects and improve the MDR reversal property.[23]

Moreover, 1,4-DHP is one of the important chemical nucleuses which are incorporated in the synthesis of new antimicrobial agents. Many 1,4-DHP compounds showed different patterns of antimicrobial activity against different types of bacteria[24] and fungi.[25,26] Some compounds disclosed activity against gram-positive bacteria and have no effect on gram-negative ones.[27] Symmetric 1,4-DHP analogues were more effective against gram-positive bacteria than gram-negative ones.[28] Patients with cancer may have a higher risk of infection because of changes in the immune system that control their body's defence systems. Cancer and cancer treatments can affect the immune system and other body systems in different ways.[29–31] Therefore, it is desirable that drugs used in the treatment of cancer have an effective impact on the prevention or treatment of secondary microbial infection.[32–34] Consequently, we have designed and synthesised two series of 1,4-DHP derivatives as potential anticancer agents with the privilege of having antimicrobial activity.

2. Rationale design

Recently, the nitrile group has become increasingly relevant in medicinal chemistry.[35] Since 2010, the US Food and Drug Administration (US FDA) has authorised at least one nitrile-containing drug per year, with five drugs approved in 2020[36]. Chronic myeloid leukaemia, breast cancer, fungal infection, and other clinical disorders are all targeted by these marketed drugs having a nitrile moiety. Nitrile-containing drugs may have greater pharmacokinetic and pharmacological effects than other pharmaceuticals with similar therapeutic effects due to the unique physicochemical

features of the nitrile group.[35–37] The second-generation EGFR kinase inhibitors, including Neratinib and Pelitinib, and compound **III**, are nitrile-containing tyrosine kinase inhibitors,[38] as illustrated in Figure 2. The majority of these inhibitors have electrophilic Michael-acceptor moieties that may interact covalently with cysteine amino acid at the lip of the EGFR's ATP binding cleft, inactivating the protein.[39,40] Additionally, the following are some pharmacophoric features shared by all EGFR-inhibitors: (i) The presence of a hetero aromatic system in the adenine binding pocket. (ii) Inserting the hydrophobic terminal head in the hydrophobic area I. (iii) The amino group which has the potential to establish significant hydrogen bonds with amino acid residues in the linker region. (iv) A hydrophobic tail that is found in hydrophobic region II.[41,42] Concerning Verapamil, Febuxostat, and compound **IV**,[43,44] the nitrile moiety partakes a notable effect as a P-gp modulator.[45,46] Additionally, 5-oxo-hexahydroquinoline bearing the pyridyl alkyl carboxylate moieties at position 3 are better inhibitors of P-gp than the compounds having carboxamide substituents that give good P-gp modulators. Alkyl and hetero aromatic insertions at the C4 position would reduce activity, whereas lipophilic aromatic insertions of CN, NO_2, and halogens groups would increase MDR reversal activity because of their electron-withdrawing substitutions.[47] The integration of the hydrophobic tail, central nitrogenous heterocycle, and hydrophobic head alongside the nitrile group were the key to build up our target compounds with dual activity via matching the pharmacophoric properties of kinases inhibitors and p-gp modulators, as verified in Figure 2. Relying on the aforementioned outcomes, we have designed 1,4-dihydropyridine derivatives comprising the nitrile group (**1a-h** and **2a-l**) as dual inhibitors of kinases and p-gp (Figure 2).

It was also found that the nitrile group connected to the dihydropyridine has an effective role as an antimicrobial.[48–52] Several novel series of nitrile-containing antimicrobial compounds with weakly basic amines are reported, which have reduced the potential for hERG (human ether-a-go-go gene) channel inhibition.[53]

3. Results and discussion

3.1. Chemistry

Two novel series of 1,4-DHP derivatives were designed and synthesised. The first series comprised eight symmetric achiral 1,4-DHPs, while the second series enclosed twelve asymmetric chiral 1,4-DHPs. The first series, eight symmetric achiral 1,4-DHPs **1a-h**, was synthesised by the classical Hantsch reaction for direct synthesis of symmetric 1,4-DHP[54] via the classical Hantsch reaction between 3-cyanobenzaldehyde, acetoacetic esters, and ammonium acetate as illustrated in Scheme 1.
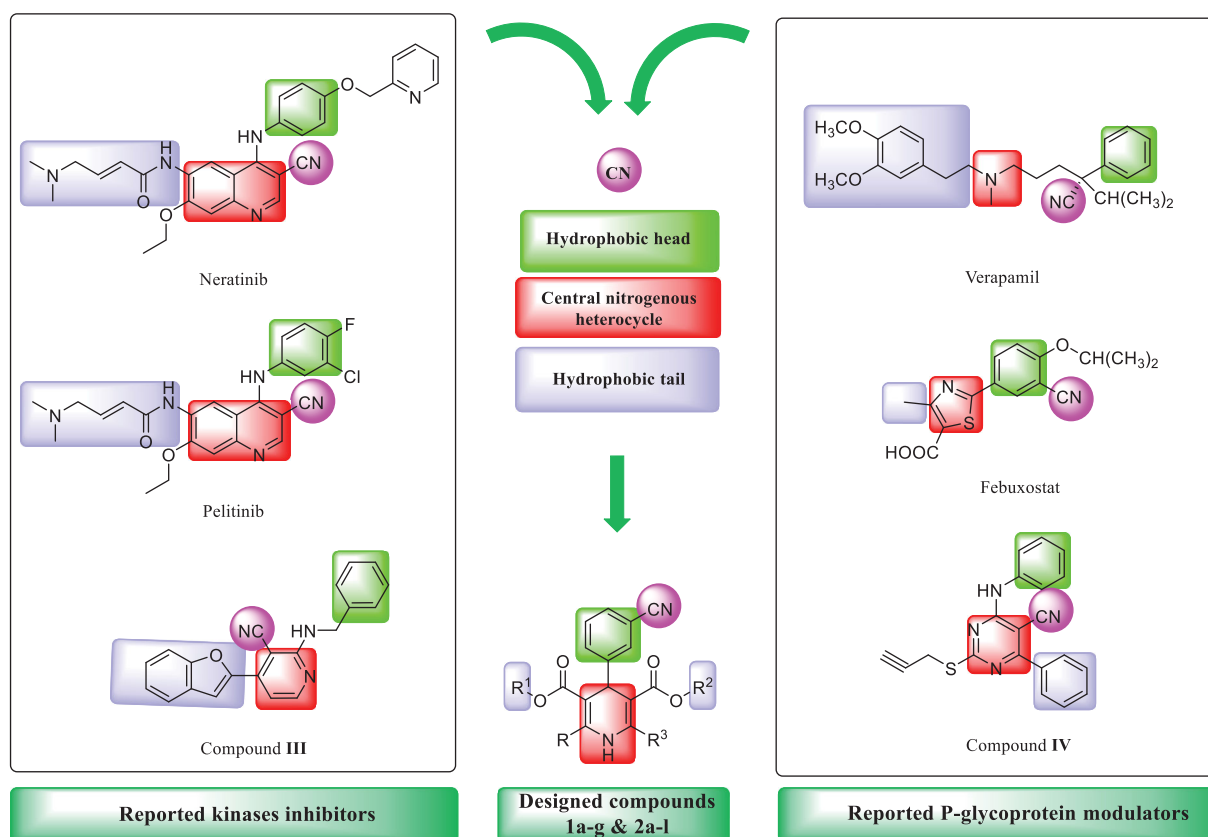
Figure 2. The rationale for the molecular design of the target compounds as kinases and P-gp dual inhibitors.

Code	R	R¹	Code	R	R¹
1a	Methyl	CH₃	1e	Methyl	H₃C—C(CH₃)—CH₃
1b	Methyl	CH₂CH₃	1f	Methyl	CH₂CH₂—O—CH₃
1c	Methyl	CH(CH₃)CH₃	1g	Methyl	CH₂—phenyl
1d	Methyl	CH₂CH(CH₃)CH₃	1h	Propyl	CH₃
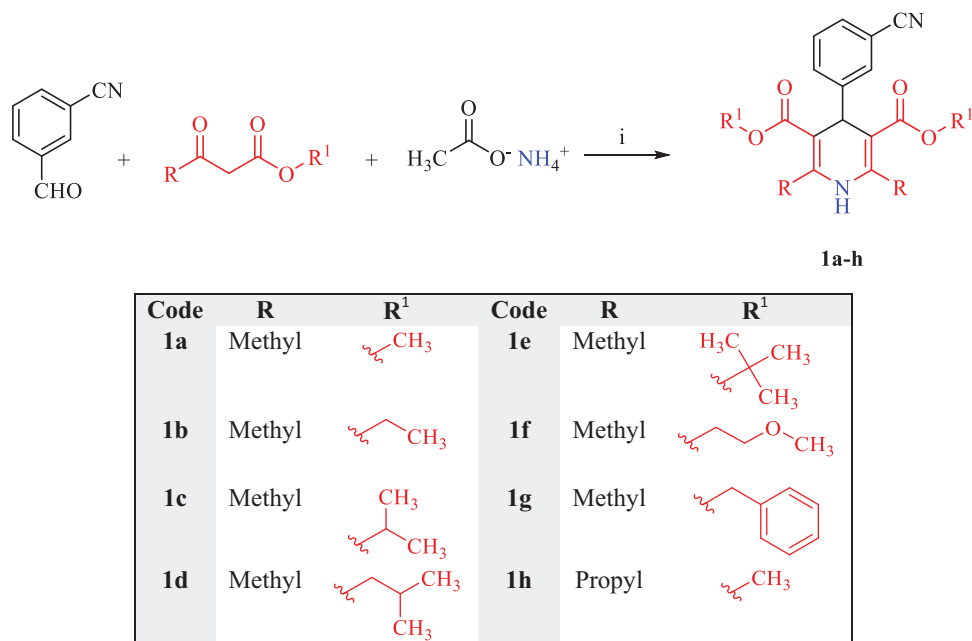
Scheme 1. Synthesis of the first series of symmetric achiral 1,4-DHP compounds, **1a-h**. Reagents and conditions: (i) MeOH, heat under reflux, 24 h.

The second series, twelve asymmetric chiral 1,4-DHPs **2a-l**, was synthesised *via* Iwanami reported method[55,56] through cyclocondensation of 3-cyanobenzaldehyde, acetoacetic esters, and alkyl 3-aminocrotonates as revealed in Scheme 2. Compounds **2a-l** were prepared as racemic mixtures.

Chemical structures of target compounds were confirmed by elemental analysis, ^{1}H, ^{13}C NMR, and mass spectroscopy. ^{1}H NMR spectra showed characteristic peaks for each proton in the synthesised compounds, as reported in the experimental section. ^{1}H NMR spectra of target compounds were characterised by two
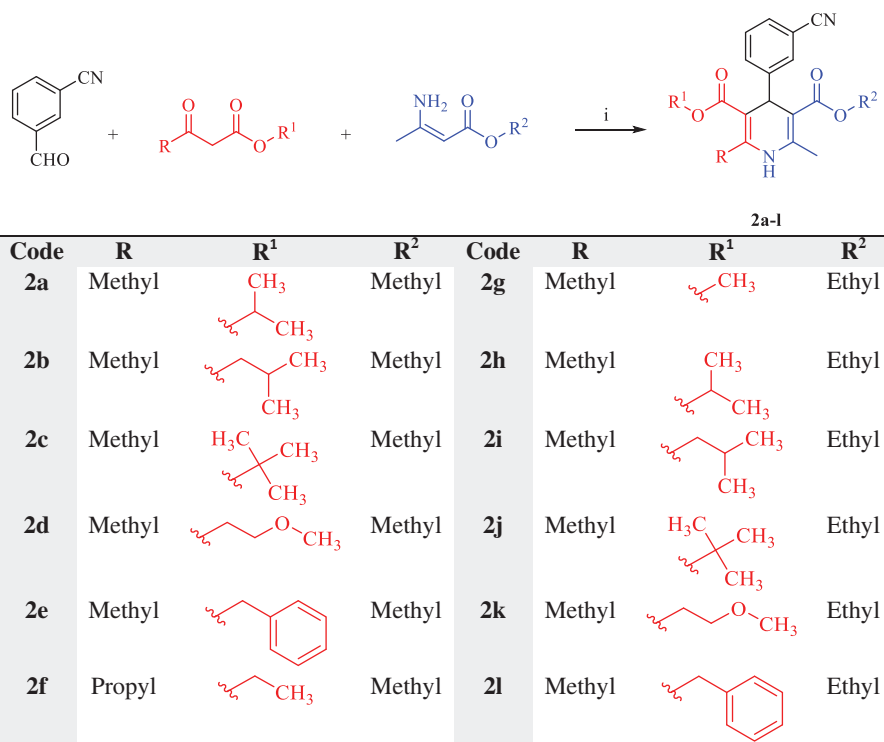
Scheme 2. Synthesis of the second series, asymmetric chiral 1,4-DHP analogues **2a-l**. Reagents and conditions: (i) MeOH, heat under reflux, 24 h.

singlet signals of C_4-H and NH protons in the 1,4-DHP ring at δ 4.88–5.09and δ 5.59–6.10 ppm, respectively. Meanwhile, the disappearance of singlet corresponding to -CHO proton of 3-cyanobenzaldehyde, as well as the singlet signal of active methylene protons in β-ketoesters, were established. ^{13}C NMR spectroscopy was performed on selected compounds, **1f**, **1g**, **1h**, **2b**, **2j**, and **2l**, which exposed the characteristic peaks for each carbon as given in the experimental section.

3.2. Pharmacological evaluation of target compounds

3.2.1. Anticancer activity

3.2.1.1. In vitro anticancer screening at NCI-USA. All target compounds were selected and submitted to the National Cancer Institute (NCI; www.dtp.nci.nih.gov), Bethesda, Maryland, USA, relying on the diversity of structures and computer modelling techniques for the assessment of their anticancer activity. The 20 compounds were screened at a single dose of 10 μM concentration against sixty cell lines of nine different types of human tumours, including leukaemia, non-small cell lung cancer, colon cancer, central nervous system cancer, melanoma, ovarian cancer, renal cancer, prostate cancer, and breast cancer, according to NCI developmental therapeutics programme.[57,58]

3.2.1.1.1. In vitro single dose (10μM) anticancer screening on NCI 60 cancer cell lines. Target compounds were subjected to in vitro NCI anticancer assay at 10 μM concentration. According to 48h drug exposure protocol, the tested compound was exposed to the cultures. Endpoint determinations were performed using a sulforhodamine B (SRB) assay to assess cell growth and viability. The results of all tested compounds were reported as a mean graph of the percentage growth (G%) of the tested cells compared to the unprocessed control cells and relative to the time zero number of cells[10] (see supplementary material) and displayed as percentage

growth inhibition (GI%) caused by the tested compounds as shown in Table 1. GI% value was calculated by subtracting the corresponding G% value from 100.

Inspecting the data illustrated in Table 1 revealed that the tested compounds exposed different profiles of antiproliferative activity. Compound **2l,** mean GI%=64, exhibited strong anticancer activity, while **1g** and **2e** showed moderate activity, mean GI%=41 and 28, respectively. Other compounds showed weak to very weak activity, exhibiting a mean GI% value below 20. Compound **2l** showed the most significant antiproliferative activity relative to other synthesised compounds. Analogue **2l** retained broad-spectrum antitumor activity against all subpanels of all tested 60 cancer cell lines. Compounds **1g** and **2e** also possessed broad-spectrum antitumor activity, but against only 56 and 49 subpanels, respectively. Compound **2l** showed excellent growth inhibitory activity against leukaemia (HL-60(TB) and K-562), non-small cell lung cancer (NCI-H522), colon cancer (HCT-116 and HT29), CNS cancer (SF-295), melanoma (M14), and breast cancer (MDA-MB-468) with GI% of 83, 83, 90, 86, 88, 84, 85, and 84, respectively. In terms of lethality, **2l** was the only compound displaying the lethal effect against only 3 subpanels: CNS cancer (SNB-75), melanoma (MDA-MB-435), and renal cancer (A498) with GI%=104, 110, and 104, respectively.

3.2.1.1.1.1. Structure–activity relationship (SAR) relying on the results of anticancer screening on NCI 60 cancer cell lines
The second series of asymmetric chiral analogues **2a-l**, mean GI% ranged from −2 to 64, exposed to better anticancer activities than symmetric achiral compounds **1a-h**, mean GI% ranged from −4 to 41, in the first series.

1. Concerning the first series of symmetric 1,4-DHPs **1a-h**, the existence of benzyl esters at both C3 and C5 of 1,4-DHP ring in **1g**, mean GI% = 41, enriched anticancer activity and

Table 1. *In vitro* cytotoxic activity, GI%, for compounds **1a-h** and **2a-l** towards 60 subpanel cancer cell lines at 10 μM concentration.

Subpanel/ Cell line	1a	1b	1c	1d	1e	1f	1g	1h	2a	2b	2c	2d	2e	2f	2g	2h	2i	2j	2k	2l
Leukaemia																				
CCRF-CEM	–	–	–	32	16	–	54	24	–	–	–	–	37	–	–	–	–	–	–	74
HL-60(TB)	–	13	29	30	41	10	62	–	23	18	–	–	43	11	–	–	–	19	12	83
K-562	–	43	25	44	34	–	69	31	16	15	–	–	56	–	–	–	24	17	10	83
MOLT-4	–	–	17	57	39	–	68	38	16	16	–	–	56	14	–	11	21	17	–	68
RPMI-8226	–	–	17	35	39	–	65	34	–	–	12	–	52	12	–	–	–	12	–	67
SR	–	48	18	52	42	–	57	32	–	29	15	–	33	–	14	–	23	22	13	78
Non-small cell lung cancer																				
A549/ATCC	–	–	11	25	20	–	45	21	–	–	–	–	31	–	–	–	10	11	–	65
EKVX	–	–	–	27	20	–	50	21	–	12	–	–	26	–	–	–	29	10	–	62
HOP-62	–	–	–	12	–	–	10	–	–	–	–	–	16	–	–	–	–	–	–	54
HOP-92	–	10	NT[b]	37	30	–	42	29	–	17	10	–	12	–	–	–	18	–	NT[b]	49
NCI-H226	–	–	–	25	22	–	46	26	–	10	–	–	31	–	–	–	22	–	–	41
NCI-H23	–	–	–	14	13	–	23	–	–	–	–	–	–	–	–	–	24	–	–	37
NCI-H322M	–	–	–	–	–	–	15	–	–	–	–	–	–	–	–	–	–	–	–	30
NCI-H460	–	–	–	13	–	–	64	–	–	–	–	–	64	–	–	–	–	–	–	77
NCI-H522	–	12	11	21	17	–	46	20	14	15	–	–	24	–	–	–	13	13	–	90
Colon cancer																				
COLO 205	–	–	–	–	–	–	47	–	–	–	–	–	43	–	–	–	–	–	–	65
HCC-2998	–	–	–	–	–	–	–	–	–	–	–	–	–	–	–	–	–	–	–	29
HCT-116	–	11	13	32	35	–	76	30	–	18	–	–	71	11	–	–	23	13	–	86
HCT-15	–	23	10	31	19	–	72	17	–	–	–	–	66	–	–	–	30	–	–	77
HT29	–	–	–	12	13	–	48	12	–	–	–	–	31	–	–	–	–	–	–	88
KM12	–	27	–	24	11	–	45	–	–	–	–	–	39	–	–	–	–	–	–	74
SW-620	–	–	–	–	–	–	65	–	–	–	–	–	45	–	–	–	–	–	–	70
CNS cancer																				
SF-268	–	–	–	25	11	–	38	22	–	–	–	–	23	–	–	–	–	–	–	42
SF-295	–	–	–	32	27	–	56	11	–	18	–	–	44	–	–	–	31	–	–	84
SF-539	–	–	–	12	10	–	35	14	–	–	–	–	32	–	–	–	–	–	–	76
SNB-19	–	–	–	–	–	–	32	–	–	–	–	–	32	–	–	–	–	–	–	58
SNB-75	24	38	20	32	38	14	23	42	–	22	27	15	34	37	–	15	18	22	–	104
U251	–	–	–	21	–	–	49	–	–	–	–	–	46	–	–	–	–	–	–	58
Melanoma																				
LOX IMVI	–	–	–	10	10	–	65	–	–	–	–	–	61	–	–	–	20	–	–	64
MALME-3M	–	–	–	–	–	–	32	–	–	–	–	–	24	–	–	–	–	–	–	62
M14	–	–	–	–	–	–	35	–	–	–	–	–	15	–	–	–	–	–	–	85
MDA-MB-435	–	42	–	–	–	–	36	–	–	–	–	–	35	–	–	–	–	–	–	110
SK-MEL-2	–	–	–	14	–	–	19	–	–	–	–	–	–	–	–	–	–	–	–	75
SK-MEL-28	–	–	–	–	–	–	34	–	–	–	–	–	27	–	–	–	–	–	–	48
SK-MEL-5	–	–	–	17	14	–	55	31	–	–	–	–	37	–	–	–	12	–	–	45
UACC-257	–	–	–	17	16	–	36	–	–	–	–	–	21	–	–	–	–	–	–	44
UACC-62	–	20	14	23	26	–	38	19	–	21	–	–	37	21	–	–	27	10	–	66
Ovarian cancer																				
IGROV1	–	–	–	–	–	–	45	10	–	12	–	–	36	–	–	–	–	–	–	57
OVCAR-3	–	–	–	10	–	–	23	–	–	–	–	–	–	–	–	–	–	–	–	76
OVCAR-4	–	–	–	16	–	–	33	32	–	–	–	–	–	–	–	–	12	–	–	28
OVCAR-5	–	–	–	–	–	–	19	–	–	–	–	–	21	–	–	–	–	–	–	38
OVCAR-8	–	–	–	11	–	–	41	–	–	–	–	–	34	–	–	–	–	–	–	51
NCI/ADR-RES	–	–	–	20	–	–	45	18	–	–	–	–	25	–	–	–	22	10	–	77
SK-OV-3	–	–	–	–	–	–	–	–	–	–	–	–	–	–	–	–	–	–	–	24
Renal cancer																				
786-0	–	–	16	18	18	–	32	16	–	–	–	–	22	–	–	–	11	13	–	63
A498	–	–	–	17	–	–	21	18	11	–	–	12	10	–	–	16	–	–	21	104
ACHN	–	–	–	16	14	–	52	–	–	–	–	–	28	–	–	–	–	–	–	52
CAKI-1	–	31	19	38	32	–	56	30	11	28	15	–	27	18	–	15	35	17	–	67
RXF 393	–	10	–	42	33	–	36	18	–	–	–	–	14	–	–	–	30	–	–	55
SN12C	–	–	–	10	–	–	32	–	–	–	–	–	–	–	–	–	–	–	–	63
TK-10	–	–	–	–	–	–	–	–	–	–	–	–	–	–	–	–	–	–	–	16
UO-31	–	13	–	20	25	–	34	19	–	11	–	–	–	13	–	–	–	–	–	56
Prostate cancer																				
PC-3	–	20	29	57	48	–	76	47	16	22	18	–	51	23	–	12	29	18	–	66
DU-145	–	–	–	–	–	–	26	–	–	–	–	–	15	–	–	–	–	–	–	42
Breast cancer																				
MCF7	–	15	11	39	34	–	53	25	–	15	13	–	29	–	11	–	34	–	–	78
MDA-MB-231	–	–	–	17	14	–	37	–	–	–	–	–	30	–	–	–	–	–	–	47
HS578T	–	16	–	25	–	–	35	18	–	14	–	–	28	–	10	–	13	–	–	59
BT-549	–	–	–	–	–	12	–	14	–	–	–	–	–	–	–	–	–	–	–	68
T-47D	–	23	30	54	53	–	53	32	–	25	12	–	11	–	–	–	32	–	–	72
MDA-MB-468	–	22	22	30	27	13	62	20	–	–	–	–	33	–	–	20	24	10	–	84
Mean GI%	−4	8	6	19	14	−1	41	14	0	5	0	−2	28	1	−1	0	9	4	−1	64

[a]Only GI% ≥ 10 are shown. GI% values of 60–100 are shown in blue colour whereas that of >100 are shown in red colour. [b]NT: not tested.
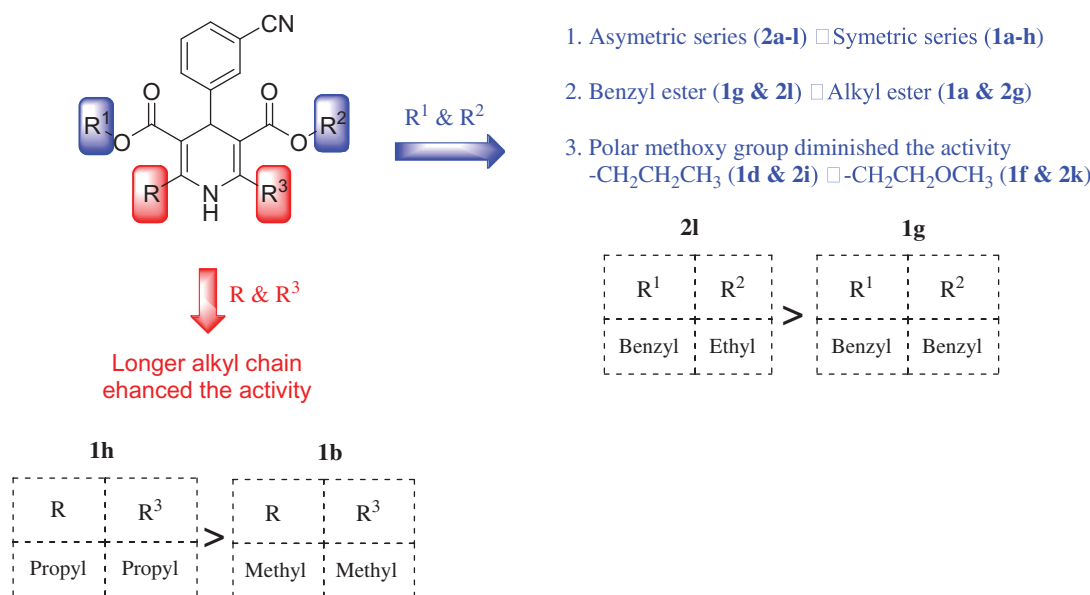
Figure 3. Summary of SAR for anticancer activity of target compounds besides structures of the most active analogues.

Table 2. Cytotoxicity, $IC_{50}{}^a$, of compounds **1g**, **2e**, and **2l** against human HCT-116 and HCT-116/ADR cells and their potentiation of DOX cytotoxicity in drug-resistant HCT-116/ADR cells.

Compound	HCT-116	HCT-116/ADR	HCT-116/ADR (DOX)	RF^b
1g	0.99 ± 0.58	10.61 ± 0.10	0.72 ± 0.001	23.48
2e	1.27 ± 0.42	29.41 ± 0.45	2.20 ± 0.015	7.68
2l	1.11 ± 0.45	15.83 ± 0.13	1.68 ± 0.010	10.05
DOX^c	1.15 ± 0.43	16.91 ± 0.14	16.91 ± 0.14	1

^{a}Data are the mean of three-independent trials of triplicate experiments. ^{b}Reversal fold activity. ^{c}Doxorubicin without modulator.

presented the strongest analogue **1g**, compared to alkyl esters analogues which reported GI% = −4 - 19. Increasing the size and lipophilicity of the alkyl chain of ester groups at C3- and C5-positions improved antitumor activity in the order: **1d**, GI% = 19 > **1e**, GI% = 14 > **1b**, GI% = 8 > **1c**, GI%=6 which hold the alky groups: isobutyl, *tert*-butyl, ethyl, and isopropyl, respectively. The presence of dimethyl esters and dimethoxyethyl esters abolished the anticancer activity of analogues, **1a**, GI% = −4 and **1f**, GI% = −1, respectively.

Regarding alkyl groups at C2 and C6 of the DHP ring, elongation of the alkyl chain enhanced antitumor activity, where **1h**, GI% = 14, with two propyl groups at C2 and C6 was more active than its analogue **1b**, GI% = 8, having two methyl groups instead of propyl.

2. In the second series of asymmetric and chiral analogues, **2a-l**, the type of esters at C3 and/or C5 of the DHP ring significantly controlled the anticancer activity. The presence of benzyl ester at C3 and ethyl ester at C5 furnished the most active analogue **2l**, mean GI% = 64. Introduction of benzyl ester at C3 strongly enhanced the activity of **2e**, mean GI% = 28, as well compared to compounds bearing aliphatic esters, which revealed GI% = −2 − 9. Reducing the size and lipophilicity of alkyl esters at C3 or C5 diminished the anticancer activity in the order: **2i**, GI% = 9 > **2b**, GI% = 5 > **2j**, GI% = 4 > **2f**, GI% = 1 which have alkyl groups: isobutyl, isobutyl, *tert*-butyl, and ethyl, respectively. The methoxyethyl ester abolished the activity of **2k**, GI% = −1. Compounds **2g-l**, GI% = −1 − 64, bearing an ethyl ester group were more active than analogues **2a-f**, GI% = −2 − 28, having a methyl

ester group at C3 of DHP ring. SAR of target compounds and the most active analogues are illustrated in Figure 3.

3.2.1.2. In vitro cytotoxicity of target compounds, 1g, 2e, and 2l in human HCT-116 and HCT-116/ADR cells and their potentiation of DOX cytotoxicity in drug-resistant HCT-116/ADR cells.

The most observable difference between human breast cancer cells, HCT-116 and drug resistance HCT-116/ADR strains, is the overexpression of P-gp in resistant strains only.[59,60] Potential inhibitors of P-gp should not be recognised or effluxed by P-gp because they are not P-gp substrates. We have selected the most active anticancer target compounds, **1g**, **2e**, and **2l**, to investigate their reversal doxorubicin (DOX) effect *via* evaluating the corresponding IC_{50} of DOX and calculating reversal-folds (RF) by dividing the IC_{50} (DOX) without P-gp modulator by IC_{50} (DOX) with P-gp modulators, **1g**, **2e**, and **2l**. Compound **1g**, with two benzyl esters at C3 and C5, displayed more potential and reversal activity (IC_{50} (DOX)=0.72 μM, RF = 23.48) than analogues with one benzyl ester group, **2e** with IC_{50} (DOX)=2.20 μM, RF = 7.68, and **2l** with IC_{50} (DOX) = 1.68 μM, RF = 10.05. Accordingly, tested target compounds inhibited P-gp and significantly augmented the cytotoxic effect of DOX against the drug resistance HCT-116/ADR cancer cells, as informed in Table 2 and Figure 4.

3.2.1.3. Mechanistic insight of 1g, 2e, and 2l induced cytotoxicity.

The potent antitumor agents in this study were subjected to further studies to investigate their potential mechanism of action.[15,61] Epidermal growth factor receptor (EGFR) kinase, HER-2 kinase, and Bruton's tyrosine kinase (BTK) inhibitory activity of the most potent antitumor compounds **1g**, **2e**, and **2l** were studied, and results were demonstrated as IC_{50} (nM) (Table 3) and % potency of EGFR, HER-2, and BTK (Figure 5), and they were compared to lapatinib as a reference drug. Compound **1g** established the highest EGFR, HER-2, and BTK inhibitory activity with IC_{50} = 62.19 ± 0.76, 70.55 ± 0.63, and 60.27 ± 0.42 nM, respectively, which was higher or close to that of lapatinib with IC_{50} = 54.38 ± 0.7, 72.81 ± 0.68, and 61.47 ± 0.58 nM, respectively. In addition, compounds **2e** and **2l** displayed promising EGFR inhibitory activity with IC_{50} = 80.35 ± 1.26 (for **2e**) and 75.22 ± 0.95 (for **2l**), HER-2 inhibitory activity with IC_{50} = 76.54 ± 0.87 (for **2e**) and 81.72 ± 0.92
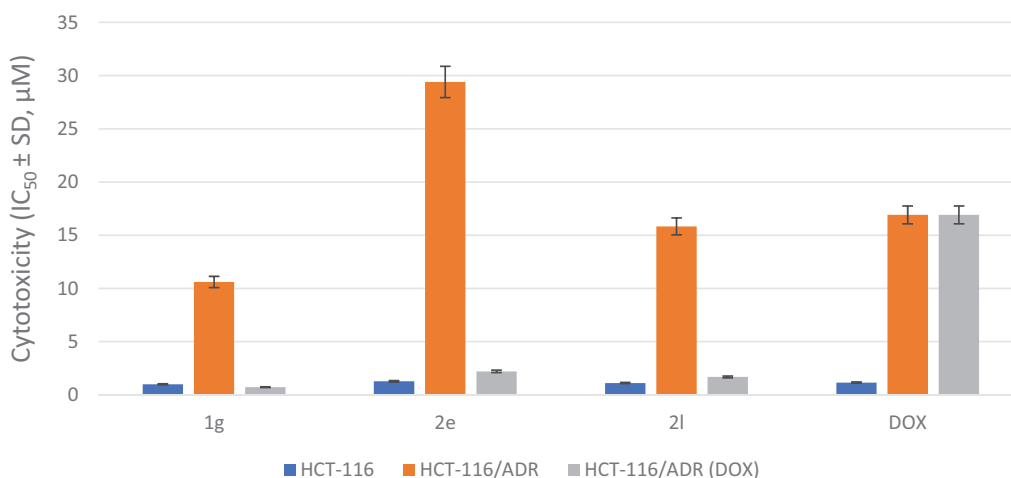
Figure 4. Cytotoxicity (μM) of compounds **1 g**, **2e**, and **2 l** on human HCT-116, HCT-116/ADR (without DOX), and HCT-116/ADR (with DOX) cells.

Table 3. Cytotoxicity (IC$_{50}$ ± SD, nM) and Potency (%)* of **1 g**, **2e**, and **2 l** on EGFR, HER-2, and BTK compared with lapatinib.

	EGFR		HER-2		BTK	
Compound	IC$_{50}$ ± SD	Potency	IC$_{50}$ ± SD	Potency	IC$_{50}$ ± SD	Potency
1g	62.19 ± 0.76	87.44	70.55 ± 0.63	103.20	60.27 ± 0.42	101.99
2e	80.35 ± 1.26	67.68	76.54 ± 0.87	95.13	82.06 ± 1.40	74.91
2l	75.22 ± 0.95	72.29	81.72 ± 0.92	89.10	63.80 ± 0.55	96.35
Lapatinib	54.38 ± 0.7	100.0	72.81 ± 0.68	100.0	61.47 ± 0.58	100.0

*Potency (%) was calculated as ((IC$_{50}$ lapatinib/IC$_{50}$ Compound) *100).

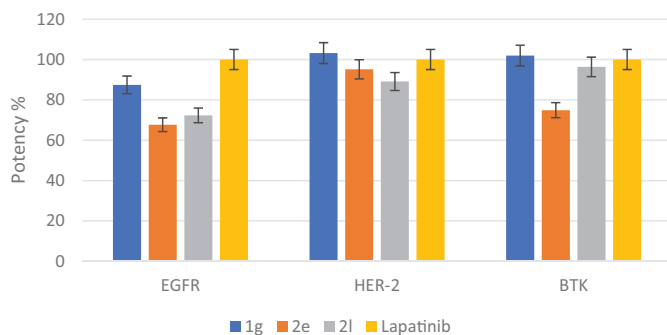**Figure 5.** % Potency of compounds **1 g**, **2e**, and **2 l** against EGFR, HER-2, and BTK.

(for **2l**), and BTK inhibitory activity with IC$_{50}$ = 82.06 ± 1.40 (for **2e**) and 63.80 ± 0.55 (for **2l**).

3.2.1.4. Annexin V–FITC apoptosis assay. Apoptosis induction is the most important mechanism by chemotherapeutics killing tumour cells.[62,63] Phosphatidylserine (PS) is translocated from the inside to the outside of the plasma membrane during apoptosis, causing cellular alterations. Annexin-V binds to PS and can be employed as a sensitive probe on the plasma membrane's outer side.[64,65] We used the annexin V–fluorescein isothiocyanate (FITC)/propidium iodide (AV/PI) dual-staining test with the BD FACS Calibur to discriminate apoptosis from necrosis in colon cancer HCT-116 cells (the most affected cancer cell lines when treated with analogues **1g**, **2e,** and **2l** at the NCI) death mediated by the most active compounds **1g**, **2e**, and **2l** (BD Biosciences, San Jose, CA).

HCT-116 cells were stained with AV/PI for 24h at a mixed molar concentration of 10 μM with each of compounds **1g**, **2e**, and **2l**.

The results of treating HCT-116 cells with each of compounds **1g**, **2e**, and **2l** for 24h were shown in Figures 6 and 7.

The early apoptosis ratio (Figure 6, lower-right quadrant of cytogram) increased from 0.81% in the control sample (dimethyl sulphoxide [DMSO]) to the range 4.37–6.17%, whereas the late apoptosis ratio (Figure 6, upper-right quadrant of cytogram) increased sharply from 0.31% to 9.45–11.28%. These findings point to an apoptotic mechanism rather than a necrotic pathway as the cause of compounds **1g**, **2e**, and **2l**-induced programmed cell death.

3.2.1.5. In vitro cell cycle analysis. Targeting the cancer cell cycle has been developed as a encouraging approach for cancer therapy.[66] DNA flow cytometry analysis was used to analyse the influence of compounds **1g**, **2e**, and **2l** on activation of the cell cycle in HCT-116 cells to determine the role of these compounds in cancer cell growth suppression and, as a result, induction of apoptosis in different phases. HCT-116 cells were treated for 24h with compounds **1g**, **2e**, and **2l** in comparison to DMSO, stained with PI, flow cytometrically evaluated, and the results were shown in Figures 8 and 9. With a concurrent reduction in the G0/G1 phase, 39.17–43.25% for compounds **1g**, **2e**, and **2l** compared to the control (57.33%), a significant rise in the proportion of apoptotic cells was found at the pre-G1 phase (15.57–19.36% on exposure to **1g**, **2e**, and **2l**) compared to control (1.65%). Furthermore, as demonstrated in Figures 8 and 9, a significant increase in cells in the G2/M phase was observed, with 26.03–31.84% for **1g**, **2e**, and **2l** and 12.52% for control, showing marked cell arrest in the G2/M phase.

3.2.2. Antimicrobial activity
3.2.2.1. In vitro antibacterial and antifungal evaluation. Target compounds were assessed in vitro for their antimicrobial activity via the agar well diffusion method[51,67] against six pathogens; two gram-positive bacteria (Staphylococcus aureus and Bacillus subtilis), two gram-negative bacteria (Escherichia coli and P. Pseudomonas aeruginosa), and two fungi (Candida albicans and Aspergillus flavus). The results of antimicrobial activity expressed as the average diameter of inhibition zone (DIZ) and the calculated % activity index (AI) for target compounds are reported in Table 4. 1,4-DHP derivatives, **1a-h** and **2a-l**, showed better inhibition activity towards Gram-positive than against Gram-negative bacteria. The second series of asymmetric 1,4-DHPs, **2a-l**, revealed DIZs = 6–22
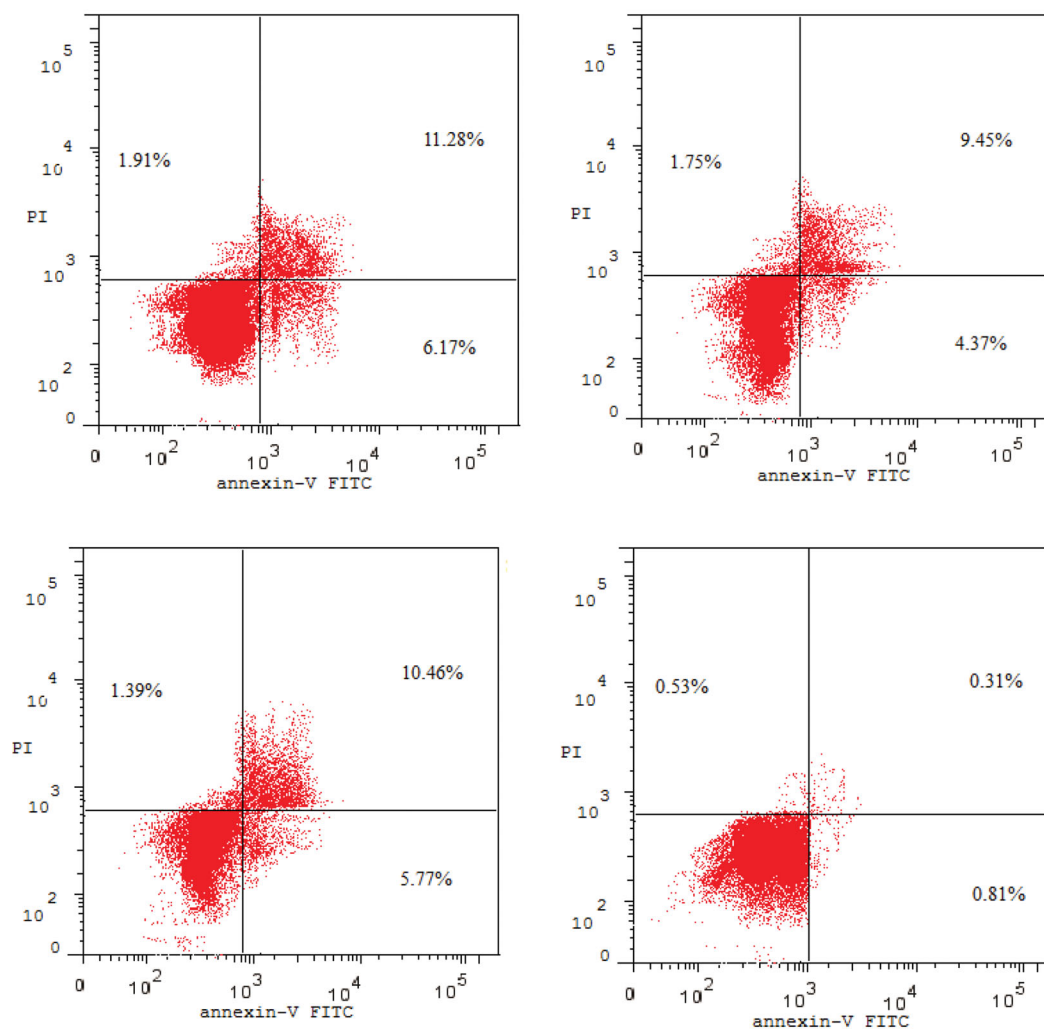
Figure 6. Apoptosis assay: Impact of compound **1 g** (upper left), compound **2e** (upper right), compound **2 l** (lower left), and DMSO (lower right) on the % of annexin V-FITC-positive staining in HCT-116 cells.
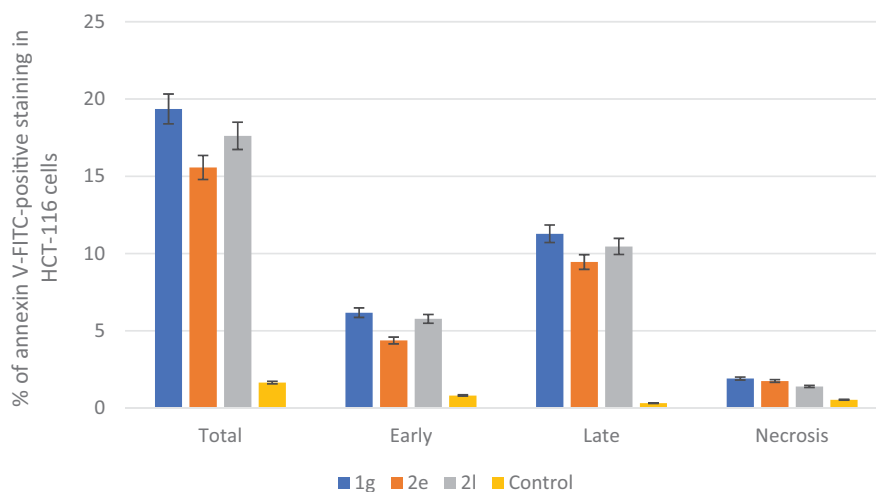

Figure 7. Effect of compounds **1 g**, **2e**, and **2 l** and DMSO on the percentage of HCT-116 cells stained positive for annexin V-FITC in apoptosis assay.

and 7–21 mm against G positive and G negative bacteria, respectively, which were better than the symmetric series of 1,4-DHPs, **1a-h** which reported DIZs = DIZs = 6–19 and 7–17 mm against G positive and G negative bacteria, respectively, while ciprofloxacin, DIZs = 23–26 mm, was used as a reference drug. Moreover, analogues **2a-l**, DIZs = 7–24 mm, displayed stronger antifungal

activity than **1a-h**, DIZs = 8–19 mm compared to clotrimazole, DIZs = 25–27 mm.

Target compounds demonstrated a higher inhibition effect against *S. aureus* than *B. subtilis* mimic the reference drug, ciprofloxacin. On the other hand, the compounds' activity was higher against *P. aeruginosa* than that against *E. coli* in contrast to
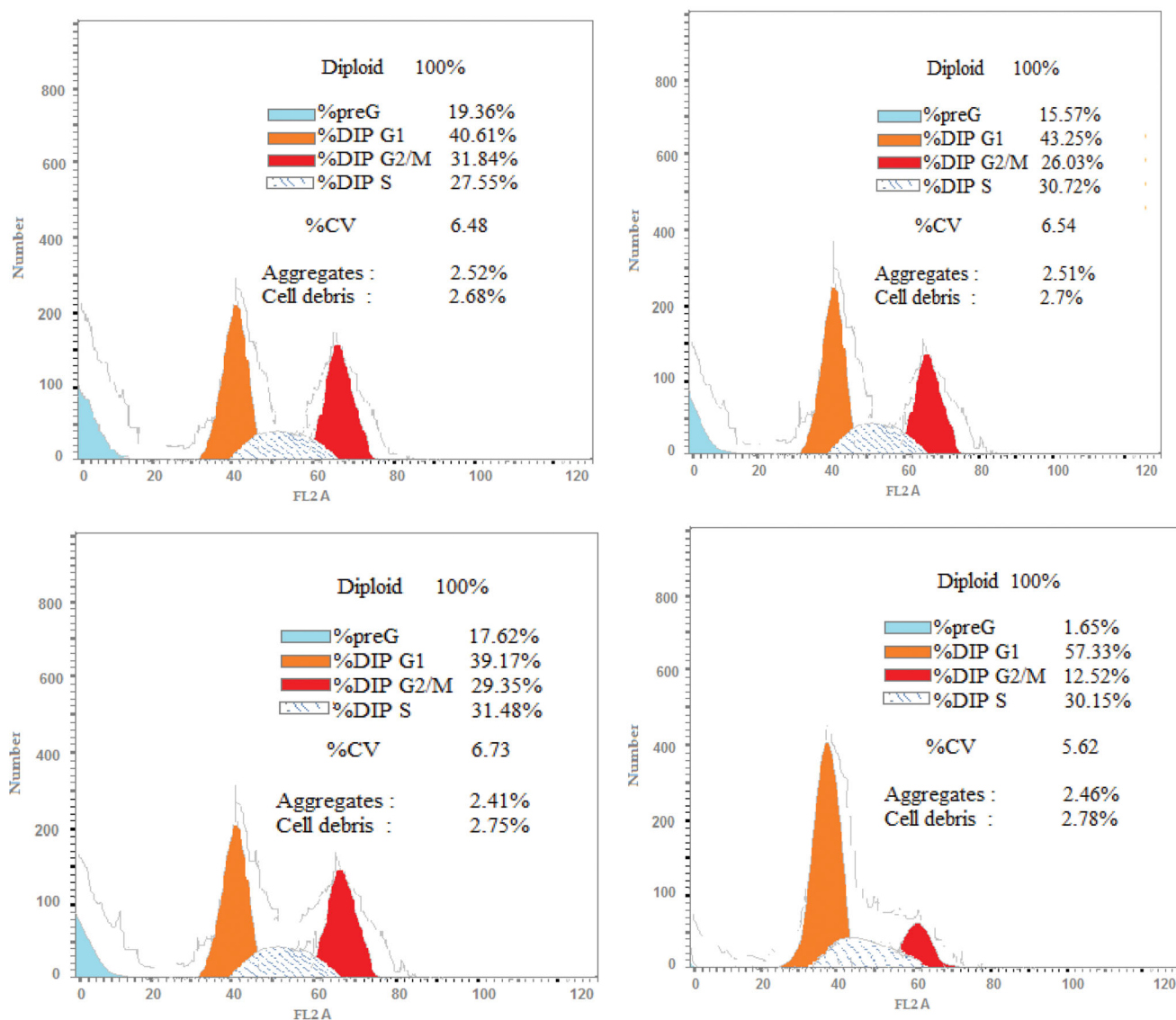
Figure 8. Cell cycle analysis of HCT-116 cells treated with compound **1 g** (upper left panel), compound **2e** (upper right panel), compound **2l** (lower left panel), and DMSO (lower right panel).
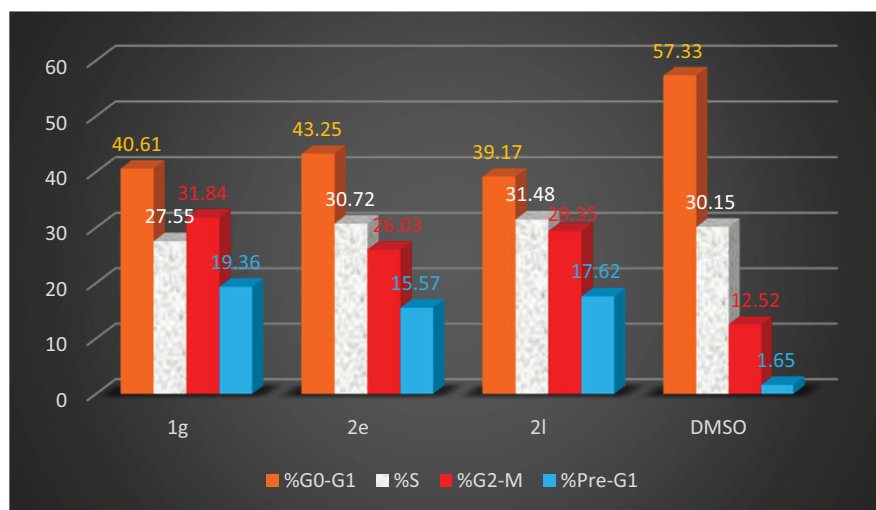

Figure 9. Outcome of compounds **1 g**, **2e**, and **2l** and DMSO on the percentage of HCT-116 cells cell cycle analysis.

Table 4. *In vitro* antimicrobial activity of compounds **1a-h** and **2a-l** against six different pathogenic strains of bacteria and fungi using agar well diffusion method.

	Diameter of inhibition zone[a] in mm (% activity index[b])					
	Bacteria				Fungi	
	G (+) bacteria		G (−) bacteria			
Compound	S. aureus	B. subtilis	E. coli	P. aeruginosa	C. albicans	A. flavus
1a	13 (54.2)	9 (39.1)	8 (30.8)	12 (52.2)	13 (48.1)	15 (60)
1b	14 (58.3)	9 (39.1)	7 (26.9)	10 (43.5)	15 (55.5)	16 (64)
1c	11 (45.8)	6 (26.1)	–	8 (34.8)	10 (37)	13 (52)
1d	–	–	–	–	–	–
1e	–	–	–	–	–	–
1f	**19 (79.2)**	**16 (69.6)**	**13 (50)**	**17 (73.9)**	**18 (66.7)**	**19 (76)**
1g	15 (62.5)	11 (47.8)	10 (38.5)	16 (69.6)	10 (37)	14 (56)
1h	7 (29.2)	–	–	–	–	8 (32)
2a	**20 (83.3)**	**17 (73.9)**	**14 (53.8)**	**19 (82.6)**	**21 (77.8)**	**22 (88)**
2b	9 (37.5)	–	9 (34.6)	13 (56.5)	7 (25.9)	11 (44)
2c	–	–	–	–	–	7 (28)
2d	15 (62.5)	10 (43.5)	10 (38.5)	14 (60.9)	12 (44.4)	15 (60)
2e	8 (33.3)	–	–	7 (30.4)	–	10 (40)
2f	6 (25)	–	–	–	–	–
2g	**22 (91.7)**	**19 (82.6)**	**19 (73.1)**	**21 (91.3)**	**23 (85.2)**	**24 (96)**
2h	11 (45.8)	8 (34.8)	–	10 (43.5)	8 (29.6)	12 (48)
2i	–	–	–	–	–	–
2j	**18 (75)**	**15 (65.2)**	**18 (69.2)**	**20 (86.9)**	**19 (70.4)**	**20 (80)**
2k	17 (70.8)	13 (56.5)	15 (57.7)	20 (86.9)	16 (59.2)	18 (72)
2l	–	–	–	–	–	–
Ciprofloxacin	24 (100)	23 (100)	26 (100)	23 (100)	NT	NT
Clotrimazole	NT	NT	NT	NT	27 (100)	25 (100)

[a]Values are means of three replicates. [b]Values below 25 are of limited value and not shown as they refer either to inactive or non-diffusing compounds.
NT: not tested.

Table 5. Antibacterial activity expressed as minimum inhibitory concentration (MIC) for analogues **1f**, **1 g**, **2a**, **2 g**, **2j**, and **2k** evaluated by the broth microdilution method.

	MIC (μg/mL)					
Compound	Bacteria				Fungi	
	G (+) bacteria		G (−) bacteria			
	S. aureus	B. subtilis	E. coli	P. aeruginosa	C. albicans	A. flavus
1f	**4**	**2**	**8**	**16**	**16**	**16**
1g	64	32	32	32	64	>64
2a	**1**	**2**	**2**	**4**	**4**	**8**
2g	**0.5**	**1**	**1**	**2**	**1**	**2**
2j	8	4	1	4	16	8
2k	16	8	4	8	32	32
Ciprofloxacin	1	2	0.5	1	NT	NT
Clotrimazole	NT	NT	NT	NT	2	1

NT: not tested.

ciprofloxacin which was more active against *E. coli*. The antifungal activity of all active compounds was higher against *A. flavus* than *C. albicans* in contrast to the reference drug, clotrimazole which was more active against *C. albicans*. Regarding the activity against Gram-positive bacteria, compounds **2a** and **2g** showed the highest inhibition effect, AI = 83 and 91 against *S. aureus,* and AI = 73 and 82 against *B. subtilis*, respectively. Compounds **1f** and **2j** showed good antibacterial activity, AI = 79 & 75 against *S. aureus*, respectively. Concerning the activity against Gram-negative bacteria, compounds **2g** and **2j** demonstrated the highest inhibition effect, AI = 91 and 86 towards *P. aeruginosa* and AI = 73 and 69 against *E. coli*, respectively. The inhibitory effect of target compounds against fungi revealed that analogues **2a**, **2g**, and **2j** presented the highest antifungal activity, AI =88, 96, and 80 towards *A. flavus* and AI = 77, 85, and 70 against *C. albicans*, respectively. Accordingly, the best antibacterial activity was observed in the presence of analogue **2g**, asymmetric DHP, and compound **1f,** symmetric DHP, towards the six tested pathogens.

We have successfully synthesised compound **1g**, which revealed a remarkable mutual activity as an anticancer (mean GI% =41) and antimicrobial agent. Analogue **1g** displayed antimicrobial effects against six different pathogenic strains of bacteria and fungi (Table 4). However, it turned out that compound **2e** (mean GI%= 28) moderately affected three pathogenic strains of bacteria and fungi. Unfortunately, the best anticancer among the series, compound **2l** (mean GI%= 64), was inactive against tested pathogenic strains (Table 4).

3.2.2.2. Determination of minimum inhibitory concentration (MIC).
The most active analogues **1f**, **1g**, **2a**, **2g**, **2j**, and **2k**, which demonstrated the strongest inhibition effect against tested pathogens, were selected for further determination of their MIC values, Table 5, *via* the microbroth dilution method.[68] Compound **2g** disclosed MIC = 0.5 and 1.0 μg/mL against G-positive bacteria, *S. aureus* and *B. subtilis*, respectively, which was two-fold more potent than ciprofloxacin, MIC = 1.0 and 2.0 μg/mL. Compound **2a** was equipotent to ciprofloxacin against both G-positive

Table 6. Docking outcomes for compounds **1 g**, **2e**, **2l**, and DOX in the active site of P-gp (PDB ID: 3G60).

Compound	Docking Score (kcal/mol)	π– π interaction		H-bond interaction		Hydrophobic interaction	
		Amino acid	Fragment	Amino acid	Fragment	Amino acid	Fragment
1g	−8.00	Phe332	Phenyl	Tyr949	C=O	Val978	Methyl (DHP)
		Phe728	Benzyl			Ala981	Benzyl Methyl (DHP)
						Val984	Benzyl
2e	−7.13	Phe332	Phenyl	———————	———————	Phe728	Methyl (DHP)
		Phe728	Benzyl			Val978	Phenyl (DHP)
2l	−7.33	Phe332	Phenyl	Tyr949	C=O	Phe974	Methyl (DHP)
		Phe728	Benzyl				
DOX	−8.21	Phe332	Anthraquinone ring	Tyr949	C=O	Leu64	Methoxy
		Phe728				Met67	Phenoxy
		Tyr949				Met68	Methoxy Phenoxy
						Phe332	Amino sugar
						Ile336	Methoxy
						Phe339	Amino sugar
						Phe974	Anthra-quinone
						Val978	Anthra-quinone

Table 7. Docking outcomes for compounds **1 g**, **2e**, **2 l**, and lapatinib in the active site of EGFR (PDB ID: 1M17).

Compound	Docking Score (kcal/mol)	π−π interaction		H-bond interaction		Hydrophobic interaction	
		Amino acid	Fragment	Amino acid	Fragment	Amino acid	Fragment
1g	−8.59	Met742	Benzyl	Cys773	C=O	Leu694	Methyl (DHP)
		Gly772	Benzyl			Val702	Phenyl
		Cys773	Benzyl			Ala719	Methyl (DHP) Benzyl
						Lys721	Benzyl
						Leu820	Methyl (DHP)
2e	−8.32	Met742	Benzyl	———————	———————	Val702	Methyl (DHP)
		Asp831	Phenyl			Ala719	Methyl (DHP) Benzyl
						Lys721	Benzyl
						Leu764	Benzyl
						Cys773	Methyl (Ester)
						Leu820	Methyl (DHP)
2l	−8.45	Met742	Benzyl	Met769	N-H	Leu694	Methyl (DHP)
						Val702	Phenyl
						Ala719	Methyl (DHP) Benzyl
						Lys721	Benzyl
						Leu768	Methyl (DHP)
						Met769	Methyl (DHP)
						Cys773	Phenyl
						Leu820	Methyl (DHP)
Lapatinib	−8.71	———	———	His781	SO_2	Leu694	Quinazoline Phenoxy
						Ala719	Phenoxy
						Lys721	Phenyl
						Met742	Phenyl
						Leu768	Quinazoline
						Phe771	SO_2
						Asp776	Alkylamine
						Tyr777	SO_2
						Glu780	Alkylamine
						His781	SO_2
						Leu820	Phenoxy

bacteria, MIC = 1.0 and 2.0 μg/mL against *S. aureus* and *B. subtilis*, respectively. The six compounds were less potent than ciprofloxacin against G-negative bacteria. Regarding activity against fungi, the most active compound, **2g**, was two-fold more potent than clotrimazole against *C. albicans*, MIC = 1.0 μg/mL. Therefore, **2g** was the most active antibacterial analogue in this series, as mentioned before. Upon all of the above findings, synthesised 1,4-DHP derivatives are promising candidates for the development of more active antibacterial and antifungal agents.

3.3. Molecular docking study

A molecular docking study was achieved on the active sites of targeted kinases and P-gp; P-gp (PDB ID: 3G60),[69] EGFR (PDB ID: 1M17),[70] HER-2 (PDB ID: 3RCD),[71] and BTK (PDB ID: 4Z3V)[72] and their alignment with co-crystalised ligand were shown in Figures S64–67. The docking results for each protein revealed that target compounds interacted with the values of the scoring functions, as reported in Tables 6–9 and Figures 10–13. Hydrophobic attraction forces and hydrogen bonds were accomplished by target compounds to engage with amino acid residues of the active sites.

3.3.1. Docking of 1g, 2e, 2l, and DOX on the active site of P-gp

Docking results exposed that compounds **1g**, **2e**, **2l**, and DOX were well located within the active site of P-gp (PDB ID: 3G60). Generally, selected analogues demonstrated π–π attraction forces; between phenyl ring and Phe332 and between benzyl group and Phe728. DOX displayed π–π attraction forces with

Table 8. Docking results for compounds **1g**, **2e**, **2l**, and lapatinib in the active site of HER-2 (PDB ID: 3RCD).

Compound	Docking Score (kcal/mol)	H-bond interaction		Hydrophobic interaction	
		Amino acid	Fragment	Amino acid	Fragment
1g	−7.72	Met801	C≡N	Leu726	Phenyl
		Arg849	N-H	Ala751	Phenyl
				Lys753	Benzyl
				Cys805	Methyl (DHP)
				Leu852	Methyl (DHP) Phenyl
2e	−7.60	————	————	Leu726	Methyl (DHP)
				Ala751	Methyl (DHP)
				Val734	Methyl (Ester)
				Lys753	Benzyl
				Leu800	Methyl (DHP)
				Met801	Methyl (DHP)
				Cys805	Phenyl
				Leu852	Phenyl
				Phe1004	Methyl (DHP)
2l	−7.51	Lys753	C=O	Leu726	Methyl (DHP) Methyl (Ester)
				Ala751	Methyl (DHP)
				Leu800	Methyl (DHP)
				Leu852	Methyl (DHP)
				Phe1004	Methyl (DHP) Methyl (Ester)
Lapatinib	−7.68	————	————	Leu726	Quinazoline Furan
				Val734	Furan Phenoxy
				Ala751	Quinazoline Phenoxy
				Lys753	Phenyl Phenoxy
				Leu796	Phenyl
				Leu800	Quinazoline
				Leu852	Quinazoline Phenyl

Table 9. Docking outcomes for compounds **1g**, **2e**, **2l**, and lapatinib in the active site of BTK (PDB ID: 4Z3V).

Compound	Docking Score (kcal/mol)	Water-mediated H-bond		H-bond interaction		Hydrophobic interaction	
		HOH no.	Fragment	Amino acid	Fragment	Amino acid	Fragment
1g	−8.50	HOH848	C≡N	Phe413	C≡N	Leu408	Benzyl
		HOH908	N-H	Lys430	C≡N	Val416	Benzyl
		HOH1041	N-H			Ala428	Benzyl
		HOH1067	C=O			Cys481	Methyl (DHP)
						Leu528	Benzyl
2e	−8.00	HOH874	OCH₂	Cys481	C=O	Leu408	Methyl (DHP) Methyl (Ester)
		HOH1021	OCH₂			Val416	Methyl (DHP)
		HOH1027	OCH₂			Leu528	Methyl (Ester) Phenyl
2l	−8.33	HOH848	C≡N	Phe413	C≡N	Leu408	Benzyl
		HOH908	N-H	Lys430	C≡N	Val416	Benzyl
		HOH1041	N-H			Ala428	Benzyl
		HOH1067	C=O			Cys481	Methyl (DHP)
						Leu528	Benzyl
Lapatinib	−8.42	HOH848	SO₂	Lys430	SO₂	Leu408	Quinazoline
		HOH1021	OCH₂	Asp539	NH	Val416	Quinazoline Furan
		HOH1027	N=C			Ala428	Furan
		HOH1033	SO₂			Cys481	Phenoxy
		HOH1158	F			Leu528	Quinazoline Furan

the same two amino acids beside Tyr949. H-bonds were observed between Tyr949 and carbonyl group in compounds **1g**, **2l**, and DOX however, it was not established by **2e**. The hydrophobicity factor played an important role in binding inhibitors within the active site, where **1g** (docking score- = −8.00 kcal/mol) displayed the best affinity to the active site among its analogues, where it formed hydrophobic interactions with Val978 & Ala981 (with methyl groups in DHP ring) besides Ala981 and Val984 (with phenyl ring). In addition, methyl groups in DHP of compound **2e** interacted with Phe728 and Val978, while the phenyl ring interacted with Val978. Besides, compound **2l** exposed hydrophobic interaction between Phe974 and methyl groups in the DHP ring. Finally, DOX (docking score = −8.21 kcal/mol) showed hydrophobic interactions with

Leu64, Met67, Met68, Ile336, Phe974, and Val978 (with anthraquinone ring and its substituents) and Phe332 and Phe339 (with sugar moiety) (Figure 10 and Table 6).

3.3.2. Docking of analogues 1g, 2e, 2l, and lapatinib on the active site of EGFR

By inspecting the binding mode of compounds **1g, 2e**, and **2l** to EGFR (docking scores = −8.59, −8.32, and −8.45 kcal/mol, respectively), a remarkable network of hydrophobic interactions was set up around the phenyl ring, benzyl and methyl groups through 5–8 amino acids. Besides, both compounds **1g** and **2l** formed H-bonds with Cys773 and Met769, respectively. The benzyl group of **1g**, **2e**, and **2l** demonstrated π–π interaction
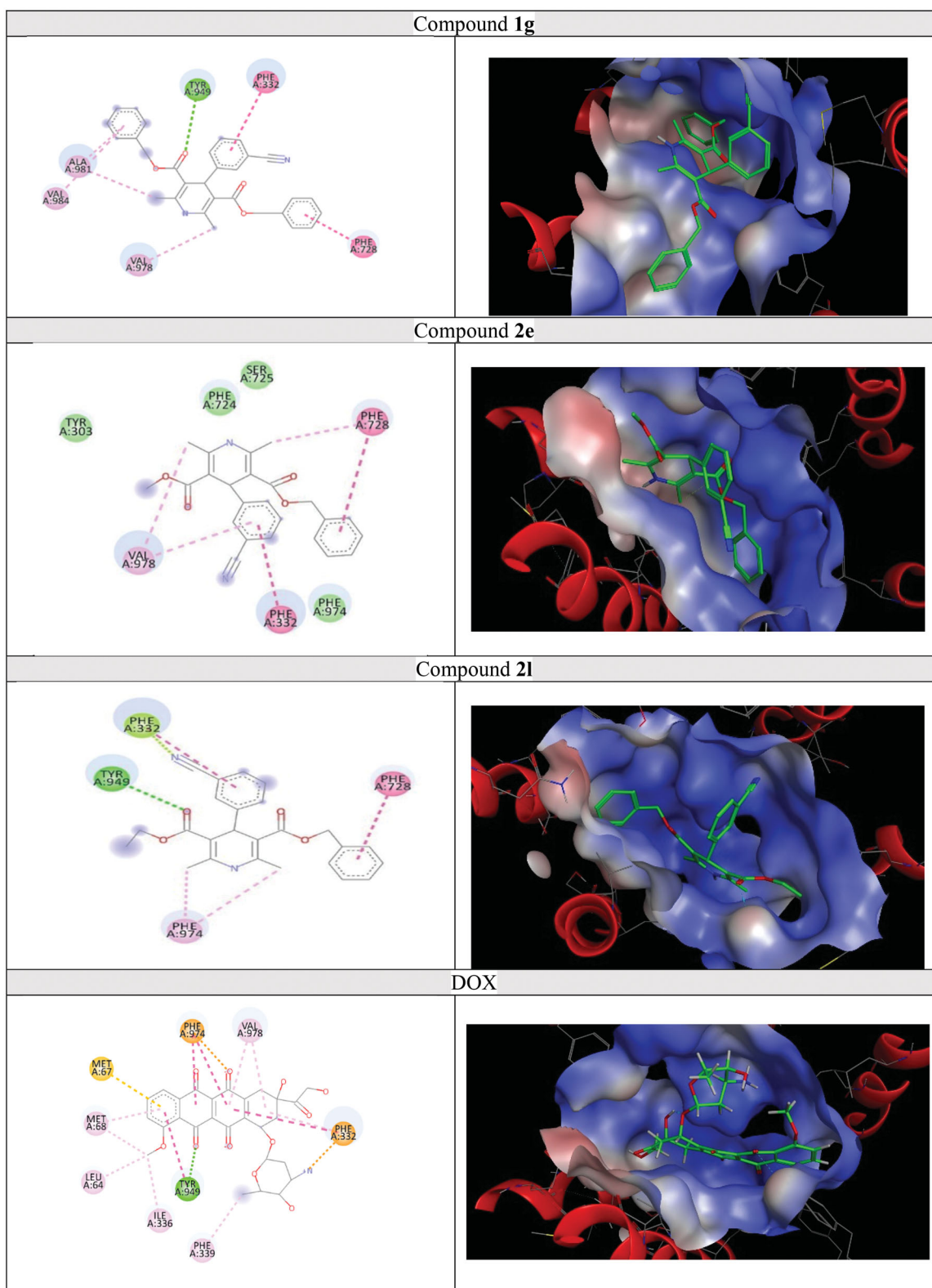
Figure 10. The 2D and 3D docking poses of compounds **1g**, **2e**, **2l** and DOX interactions with P-gp (PDB ID: 3G60).

with Met742. In addition, there were extra $\pi-\pi$ interactions observed for compound **1g** through benzyl group with Gly772 and Cys773 and in compound **2e** through phenyl group with Asp831, as declared in (Figure 11 and Table 7). In comparison to lapatinib (docking scores $=-8.71$ kcal/mol), it did not undergo $\pi-\pi$ interaction, but it still makes hydrogen bond with His781 and hydrophobic interaction with about eleven amino acids which enabled it to outperform the other compounds.
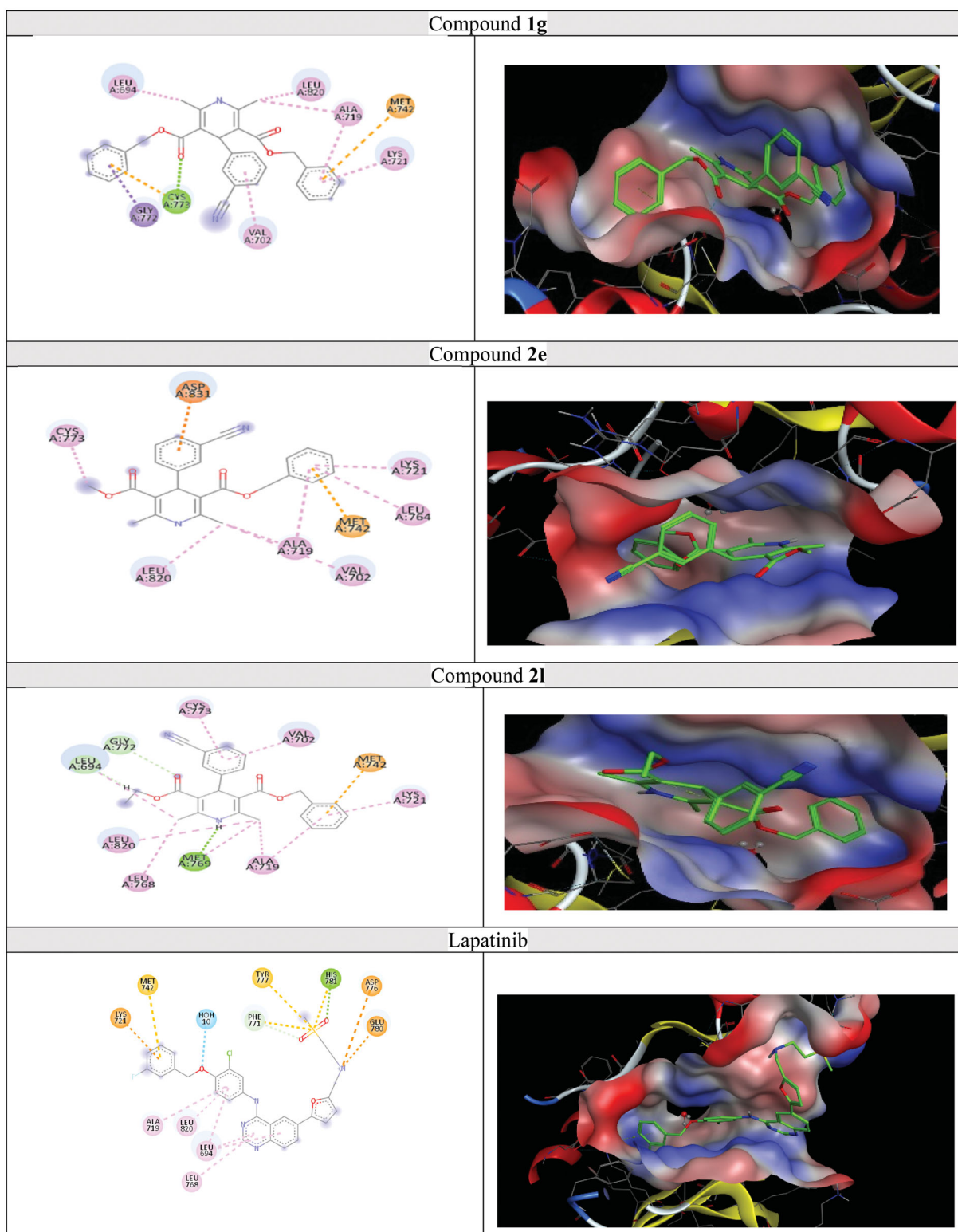
Figure 11. The 2D and 3D docking poses of compounds **1g**, **2e**, **2l** and lapatinib interactions with EGFR (PDB ID: 1M17).

3.3.3. Docking study for analogues 1g, 2e, 2l, and lapatinib on the active site of HER-2

HER-2 is overexpressed in various human malignancies, including not less than 40% of solid tumours, while its overexpression is linked to a bad prognosis. HER-2 is also an appealing target for tumour-specific therapy because it is expressed at low concentrations in normal human tissues. The normal kinase bilobed folding is adopted by HER-2.[73] When compounds **1g** and **2l** interacted with HER-2 (PDB: 3RCD), two H-bonds were observed with Met801 and Arg849 in **1g** and one H-bond with Lys753 in **2l**. But compound **2e** and lapatinib didn't interact with this target by any H-bond. Hydrophobicity of target compounds played an important role in increasing binding affinity and docking scores of **1g**, **2e**, **2l**, and lapatinib (docking scores = −7.72, −7.60, −7.51, and
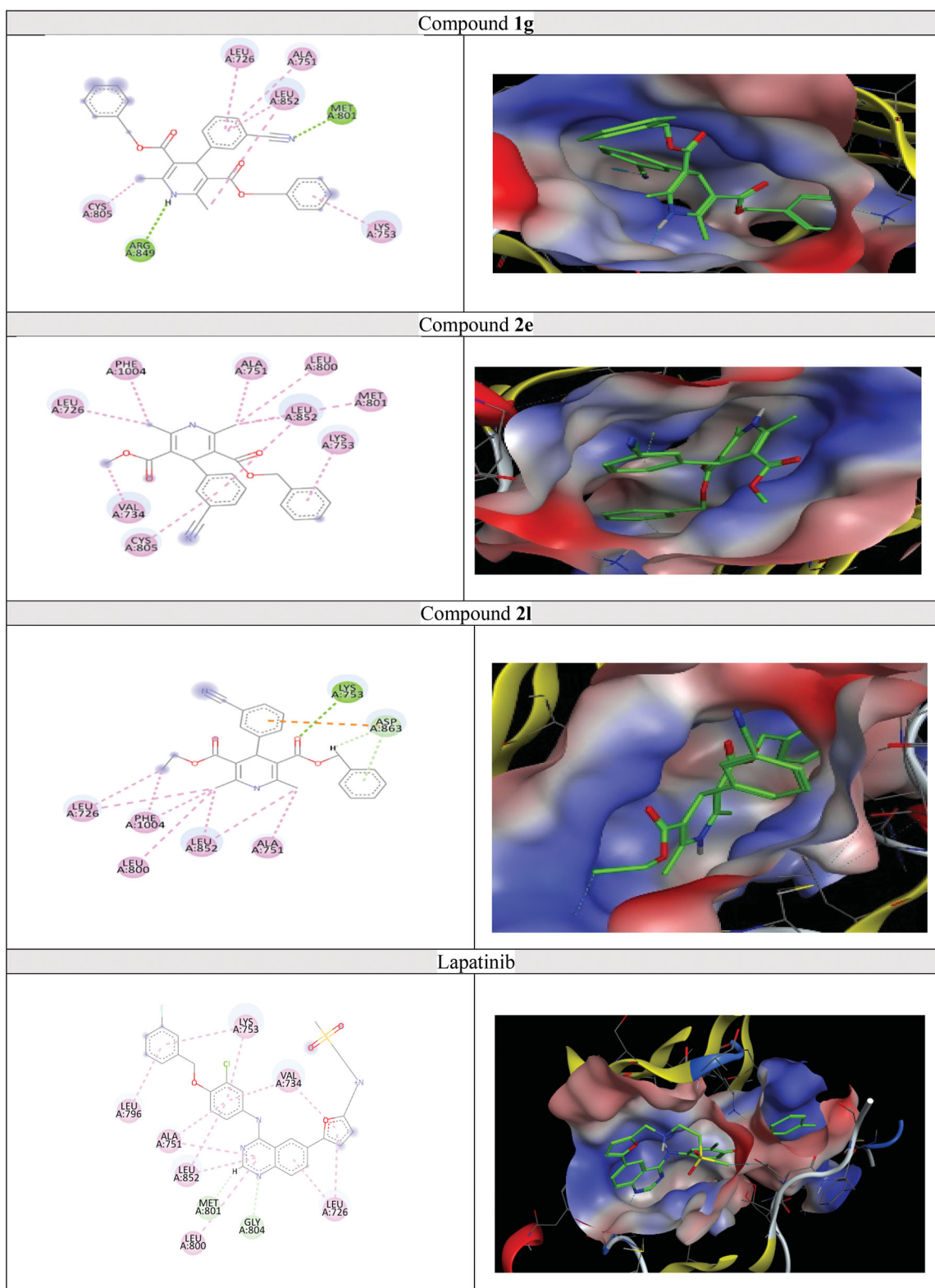
Figure 12. The 2D and 3D docking poses of compounds **1g**, **2e**, **2l** and lapatinib interactions with HER-2 (PDB ID: 3RCD).

−7.68 kcal/mol, respectively), as presented in Table 8 and Figure 12.

3.3.4. Docking of analogues 1g, 2e, 2l, and lapatinib in the active site of BTK

Several BTK mutations have been identified, which reveal the significance of specific amino acid residues in the ATP binding region (PDB: 4z3v).[74,75] The best-suited synthesised compounds, **1g** (docking score = −8.50 kcal/mol) and **2l** (docking score = −8.33 kcal/mol), were docked into the active site of BTK, where the benzyl group fitted in the hydrophobic pocket and generated network of hydrophobic attraction forces with Leu408, Val416, Ala428, and Leu528. Similarly, Cys481 sorted hydrophobic interaction with two methyl groups at C2 and C6
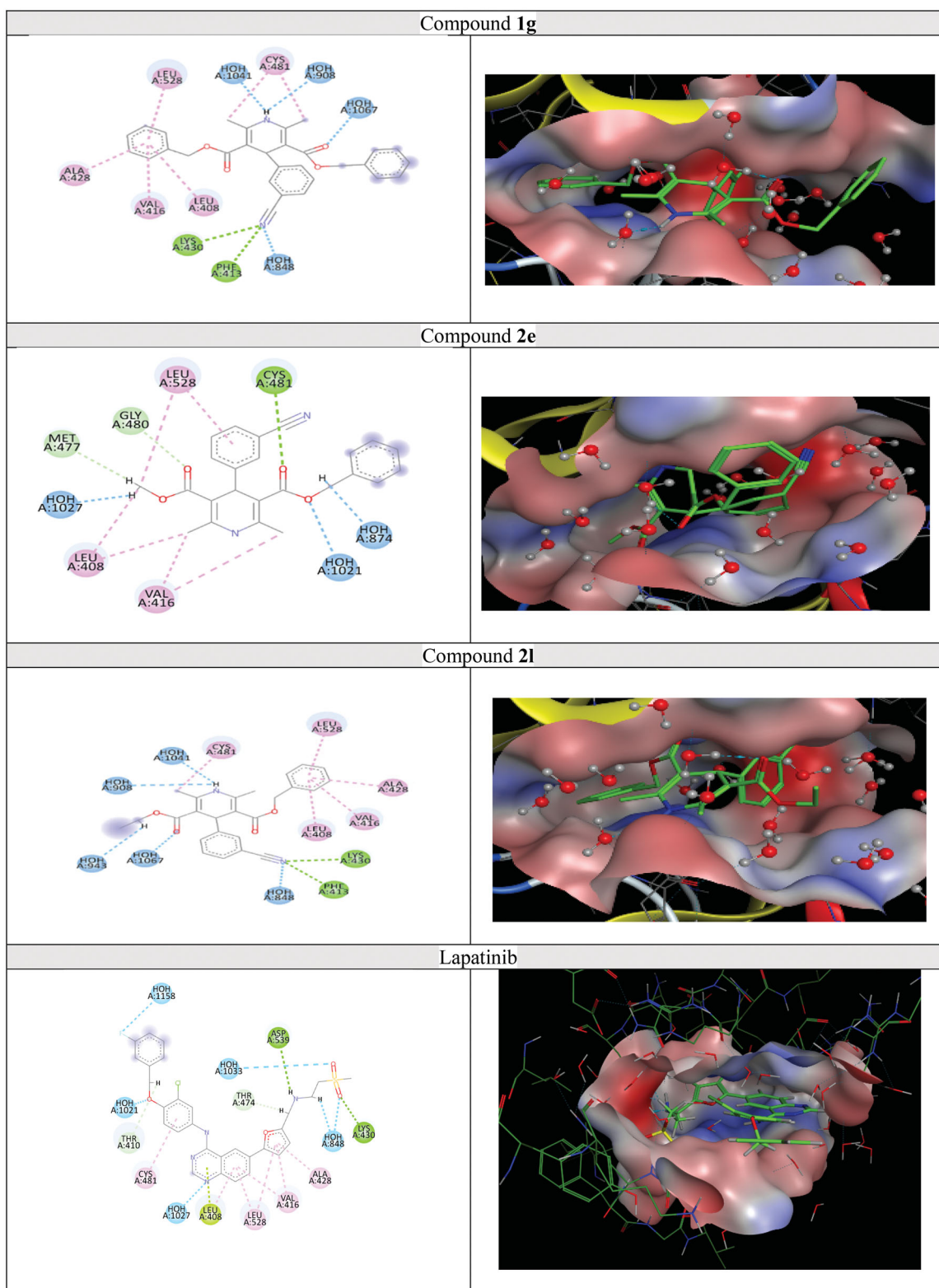
Figure 13. The 2D and 3D docking poses of compounds 1g, 2e, 2l and lapatinib interactions with BTK (PDB ID: 4Z3V).

of compound 1g while making hydrophobic interaction with only one methyl group of compound 2l. Nitrile group at 1g and 2l interact with Phe413 and Lys430 via two H-bonds. Finally, both compounds make four water-mediated H-bonds with HOH848, HOH908, HOH1041, and HOH1067, as displayed in Figure 13 and Table 9. Meanwhile, compound 2e (docking

score = −8.0 kcal/mol) displayed hydrophobic interaction through phenyl and methyl groups with Leu408, Val416, and Leu528. 2e formed one H-bond through carbonyl group with Cys481 besides three water-mediated H-bonds with HOH874, HOH1021, and HOH1027, as shown in Figure 13 and Table 9. Finally, lapatinib (docking score = −8.42 kcal/mol) displayed similar binding

interactions to compound **1g** (H-bond and hydrophobic) towards BTK.

4. Conclusion

Two new series comprised eight symmetric achiral (**1a-h**) and twelve asymmetric chiral (**2a-l**) 1,4-DHP derivatives were designed and synthesised. Chemical structures of target compounds were confirmed by elemental analysis, ^{1}H NMR, ^{13}C NMR, and mass spectroscopy. Screening of cytotoxic effect of target compounds against NCI sixty cell lines of nine different types of human tumour revealed that compounds **1g**, **2e**, and **2l** reported the best activities. EGFR, HER-2, and BTK inhibitory effects of compounds **1g**, **2e**, and **2l** were close to that of lapatinib. Annexin V–FITC apoptosis assay exposed that analogues **1g**, **2e**, and **2l** attained antiproliferative activity through apoptotic mechanism rather than a necrotic pathway. DNA flow cytometric analysis displayed that, for analogues **1g**, **2e**, and **2l,** the proportion of apoptotic cells is significantly increased at the G2/M phase; thus, they have arrested cells at the G2/M phase. Evaluation of the antimicrobial activity of the synthesised compounds revealed that compound **1g** has a remarkable effect as anticancer and antimicrobial together. Moreover, although being the greatest anticancer among the series, compound **2l** has no effect on microbial infection. Docking studies for selected compounds were performed in the active sites of crystal structures of four proteins to understand biological differences.

5. Experimental

5.1. Chemistry

All of the organic reagents used in this study were purchased from Sigma-Aldrich, Alfa Aesar, and Merck, and were utilised without additional purification. To improve the photo-stability of the products, they were prepared, collected, and purified in the dark in the absence of oxidising agents. Thin-layer chromatography (TLC) was utilised to monitor reaction courses, product mixes, and purity, utilising a pre-coated sheet with a Fluorescein indicator (Fastman Kodak Co., Silica 60 F_{254}) and shortwave UV light at 254 nm. A PuriFlash 4100 system (Interchim; Montlucon, France) was utilised to separate compound **2c** from its product combination using preparative silica gel HPLC. The system includes a mixing HPLC quaternary pump, PDA-UV–Vis detector (190–840nm), fraction collector, and sample loading module. For system control and process monitoring, Interchim Software version 5.0 was used. The column utilised was a 25g normal phase (NP) column with a particle size of 30 m silica. The **2c** product combination was diluted in 100 mL of *n*-hexane: ethyl acetate (1:1) before being dry loaded into the column with 12g of silica. To improve separation and minimise separation time, HPLC chromatography was performed in elution gradient mode, with the mobile phase composition varying from 0% to 100% v/v ethyl acetate - *n*-hexane during separation.

Compounds **2a-l** had their optical rotation (α) determined on a Polax-2L Polarimeter (ATAGO Co., Ltd., Japan) at Tanta University's Department of Pharmaceutical Chemistry, Faculty of Pharmacy, and there was no rotation. The open capillary method was utilised to measure melting points, which were not adjusted, using electro-thermal equipment (Stuart SMP10). Micro Analytical Centre, Faculty of Science, Cairo University, Giza, Egypt, used a Perkin-Elmer 2400 CHN analyser to do elemental analysis (percent C, H, and N), and all elemental analysis data were within ±0.4 of

theoretical values. Using CDCl$_3$ as a solvent, ^{1}H NMR spectra were acquired at 400 MHz on a Bruker FT-NMR spectrometer. Using CDCl$_3$ as a solvent, ^{13}C NMR spectra were acquired at 125 MHz on a JEOL ECA-500 II FT-NMR spectrometer. Chemical shifts were measured in parts per million (ppm) compared to the internal reference, tetramethylsilane (TMS). The coupling constants were expressed in hertz (Hz). Faculty of Science, Kafrelsheikh University, Egypt, conducted ^{1}H NMR spectra. Faculty of Science, Mansoura University, Egypt, conducted ^{13}C NMR spectra. In negative ion mode, electrospray ionisation mass spectra (ESI–MS) were acquired on an Advion compact mass spectrometer (CMS). Nawah Scientific Co., Al-Asmarat, Almokattam, Cairo, Egypt, performed the ESI–MS.

5.1.1. General procedure for the synthesis of symmetric compounds (1a-h)

Ammonium acetate (0.338g, 4.385 mmol) was added to a stirring solution of 3-cyanobenzaldehyde (0.500g, 3.813 mmol), and the corresponding alkyl acetoacetate (7.626 mmol) in methanol (10 mL) in a 50 mL round-bottomed flask. The reaction mixture was kept in the dark and heated under reflux for 24h. The cooled solution was stored in the refrigerator. To obtain products (**1a-h**), the crude crystals were filtered and refined *via* crystallisation from methanol.

5.1.1.1. Dimethyl 4-(3-cyanophenyl)-2,6-dimethyl-1,4-dihydropyridine-3,5-dicarboxylate (1a). Yellowish white powder, m.p. 200–202 °C.[76] ^{1}H NMR (400 MHz, CDCl$_3$) δ (ppm): 2.29 (s, 6H, C$_2$-**CH$_3$** and C$_6$-**CH$_3$**), 3.58 (s, 6H, 2 of COO**CH$_3$**), 4.95 (s, 1H, C$_4$-**H**), 5.73 (s, 1H, N**H**), 7.24 (t, J = 7.70 Hz, 1H, C$_{5'}$-**H**), 7.36 (d, J = 7.70 Hz, 1H, C$_{4'}$-**H**), 7.46 (d, J = 7.70 Hz, 1H, C$_{6'}$-**H**), 7.47 (s, 1H, C$_{2'}$-**H**). Anal. (%) for C$_{18}$H$_{18}$N$_2$O$_4$, calcd. (found), C 66.25 (66.03), H 5.56 (5.52), N 8.58 (8.61).

5.1.1.2. Diethyl 4-(3-cyanophenyl)-2,6-dimethyl-1,4-dihydropyridine-3,5-dicarboxylate (1b). Yellow powder, m.p. 144–146 °C.[76] ^{1}H NMR (400 MHz, CDCl$_3$) δ (ppm): 1.24 (t, J = 7.08 Hz, 6H, 2 of CH$_2$**CH$_3$**), 2.37 (s, 6H, C$_2$-**CH$_3$** and C$_6$-**CH$_3$**), 4.05–4.17 (m, 4H, 2 of **CH$_2$**CH$_3$), 5.03 (s, 1H, C$_4$-**H**), 5.90 (s, 1H, N**H**), 7.32 (t, J = 7.60 Hz, 1H, C$_{5'}$-**H**), 7.44 (d, J = 7.60 Hz, 1H, C$_{4'}$-**H**), 7.57 (d, J = 7.60 Hz, 1H, C$_{6'}$-**H**), 7.58 (s, 1H, C$_{2'}$-**H**). Anal. (%) for C$_{20}$H$_{22}$N$_2$O$_4$, calcd. (found), C 67.78 (67.51), H 6.26 (6.14), N 7.90 (8.00).

5.1.1.3. Diisopropyl 4-(3-cyanophenyl)-2,6-dimethyl-1,4-dihydropyridine-3,5-dicarboxylate (1c). Yield (0.400g, 27%) as yellowish white powder, m.p. 124–125 °C. ^{1}H NMR (400 MHz, CDCl$_3$) δ (ppm): 1.04 (d, J = 6.24 Hz, 6H, 2 of **CH$_3$**CHCH$_3$), 1.17 (d, J = 6.24 Hz, 6H, 2 of CH$_3$CH**CH$_3$**), 2.26 (s, 6H, C$_2$-**CH$_3$** and C$_6$-**CH$_3$**), 4.83–4.93 (m, 3H, 2 of COO**CH** and C$_4$-**H**), 5.81 (s, 1H, N**H**), 7.23 (t, J = 7.62 Hz, 1H, C$_{5'}$-**H**), 7.35 (d, J = 7.62 Hz, 1H, C$_{4'}$-**H**), 7.48 (d, J = 7.62 Hz, 1H, C$_{6'}$-**H**), 7.49 (s, 1H, C$_{2'}$-**H**). ESI–MS: *m/z* (% abundance): 382.6 (M$^+$, 25), 381.6 ([M– 1]$^+$, 100). Anal. (%) for C$_{22}$H$_{26}$N$_2$O$_4$, calcd. (found), C 69.09 (68.86), H 6.85 (6.89), N 7.32 (7.08).

5.1.1.4. Diisobutyl 4-(3-cyanophenyl)-2,6-dimethyl-1,4-dihydropyridine-3,5-dicarboxylate (1d). Yield (1.213g, 78%) as yellow powder, m.p. 146–148 °C. ^{1}H NMR (400 MHz, CDCl$_3$) δ (ppm): 0.90 (d, J = 6.78 Hz, 6H, 2 of **CH$_3$**CHCH$_3$), 0.92 (d, J = 6.78 Hz, 6H, 2 of CH$_3$CH**CH$_3$**), 1.87–1.97 (m, 2H, 2 of CH$_2$**CH**), 2.39 (s, 6H, C$_2$-**CH$_3$** and C$_6$-**CH$_3$**), 3.86 (d, J = 6.48 Hz, 4H, 2 of COO**CH$_2$**), 5.09 (s, 1H, C$_4$-**H**), 5.83 (s, 1H, N**H**), 7.33 (t, J = 7.72 Hz, 1H, C$_{5'}$-**H**), 7.45 (d, J = 7.72 Hz, 1H, C$_{4'}$-**H**), 7.58 (d, J = 7.72 Hz, 1H, C$_{6'}$-**H**), 7.59 (s, 1H,

$C_{2'}$-**H**). ESI–MS: m/z (% abundance): 410.7 (M^+, 28), 409.7 ($[M-1]^+$, 100). Anal. (%) for $C_{24}H_{30}N_2O_4$, calcd. (found), C 70.22 (69.92), H 7.37 (6.99), N 6.82 (6.52).

5.1.1.5. Di-tert-butyl 4-(3-cyanophenyl)-2,6-dimethyl-1,4-dihydro-pyridine-3,5-dicarboxylate (1e).
Yield (0.782g, 50%) as white powder, m.p. 166–168 °C. ^{1}H NMR (400 MHz, CDCl$_3$) δ (ppm): 1.41 (s, 18H, 2 of C(**CH$_3$**)$_3$), 2.32 (s, 6H, C_2-**CH$_3$** and C_6-**CH$_3$**), 4.95 (s, 1H, C_4-**H**), 5.78 (s, 1H, N**H**), 7.33 (t, $J=7.18$ Hz, 1H, $C_{5'}$-**H**), 7.44 (d, $J=7.18$ Hz, 1H, $C_{4'}$-**H**), 7.57 (d, $J=7.18$ Hz, 1H, $C_{6'}$-**H**), 7.58 (s, 1H, $C_{2'}$-**H**). ESI–MS: m/z (% abundance): 410.7 (M^+, 27), 409.7 ($[M-1]^+$, 100). Anal. (%) for $C_{24}H_{30}N_2O_4$, calcd. (found), C 70.22 (70.23), H 7.37 (7.72), N 6.82 (7.21).

5.1.1.6. Di(2-methoxyethyl) 4-(3-cyanophenyl)-2,6-dimethyl-1,4-dihydropyridine-3,5-dicarboxylate (1f).
Yield (0.589g, 37%) as white powder, m.p. 125–126 °C. ^{1}H NMR (400 MHz, CDCl$_3$) δ (ppm): 2.28 (s, 6H, C_2-**CH$_3$** and C_6-**CH$_3$**), 3.30 (s, 6H, 2 of O**CH$_3$**), 3.41–3.52 (m, 4H, 2 of **CH$_2$**OCH$_3$), 4.04–4.17 (m, 4H, 2 of COO**CH$_2$**), 4.98 (s, 1H, C_4-**H**), 5.93 (s, 1H, N**H**), 7.24 (t, $J=7.61$ Hz, 1H, $C_{5'}$-**H**), 7.35 (d, $J=7.61$ Hz, 1H, $C_{4'}$-**H**), 7.51 (d, $J=7.61$ Hz, 1H, $C_{6'}$-**H**), 7.54 (s, 1H, $C_{2'}$-**H**). ^{13}C NMR (125 MHz, CDCl$_3$) δ (ppm): 19.5 (2 C, C_2-**CH$_3$** and C_6-**CH$_3$**), 39.7 (1 C, C_4), 58.8 (2 C, 2 of O**CH$_3$**), 62.9 (2 C, 2 of **CH$_2$**OCH$_3$), 70.4 (2 C, 2 of COO**CH$_2$**), 103.1 (2 C, C_3 and C_5), 111.6 (1 C, $C_{3'}$), 119.5 (1 C, CN), 128.5 (1 C, $C_{5'}$), 129.8 (1 C, $C_{4'}$), 132.1 (1 C, $C_{6'}$), 132.9 (1 C, $C_{2'}$), 144.9 (2 C, C_2 and C_6), 149.0 (1 C, $C_{1'}$), 167.2 (2 C, COO). ESI–MS: m/z (% abundance): 414.6 (M^+, 27), 413.6 ($[M-1]^+$, 100). Anal. (%) for $C_{22}H_{26}N_2O_6$, calcd. (found), C 63.76 (63.68), H 6.32 (6.01), N 6.76 (6.81).

5.1.1.7. Dibenzyl 4-(3-cyanophenyl)-2,6-dimethyl-1,4-dihydropyridine-3,5-dicarboxylate (1g).
Yield (0.884g, 48%) as yellow powder, m.p. 162–164 °C. ^{1}H NMR (400 MHz, CDCl$_3$) δ (ppm): 2.27 (s, 6H, C_2-**CH$_3$** and C_6-**CH$_3$**), 4.93 (d, $J_{gem}=12.29$ Hz, 2H, 2 of **H**CHC$_6$H$_5$), 4.95 (s, 1H, C_4-**H**), 5.02 (d, $J_{gem}=12.29$ Hz, 2H, 2 of HC**H**C$_6$H$_5$), 5.75 (s, 1H, N**H**), 7.07–7.34 (m, 14H, 2 of **C$_6$H$_5$**, $C_{2'}$-**H**, $C_{4'}$-**H**, $C_{5'}$-**H** and $C_{6'}$-**H**). ^{13}C NMR (125 MHz, CDCl$_3$) δ (ppm): 19.7 (2 C, C_2-**CH$_3$** and C_6-**CH$_3$**), 39.6 (1 C, C_4), 65.9 (2 C, 2 of **CH$_2$**C$_6$H$_5$), 103.1 (2 C, C_3, and C_5), 111.7 (1 C, $C_{3'}$), 119.3 (1 C, CN), 128.1 (4 C, 2 of (C_2 and C_6 of C_6H$_5$)), 128.5 (6 C, 2 of (C_3, C_4' and C_5 of C_6H$_5$)), 128.5 (1 C, $C_{5'}$), 129.9 (1 C, $C_{4'}$), 131.8 (1 C, $C_{6'}$), 132.9 (1 C, $C_{2'}$), 136.0 (2 C, 2 of (C_1 of C_6H$_5$)), 145.0 (2 C, C_2, and C_6), 148.8 (1 C, $C_{1'}$), 166.7 (2 C, COO). ESI–MS: m/z (% abundance): 478.8 (M^+, 36), 477.8 ($[M-1]^+$, 100). Anal. (%) for $C_{30}H_{26}N_2O_4$, calcd. (found), C 75.30 (74.96), H 5.48 (5.18), N 5.85 (5.61).

5.1.1.8. Diethyl 4-(3-cyanophenyl)-2,6-dipropyl-1,4-dihydropyridine-3,5-dicarboxylate (1h).
Yield (0.633g, 40%) as white powder, m.p. 140–141 °C. ^{1}H NMR (400 MHz, CDCl$_3$) δ (ppm): 1.02 (t, $J=7.30$, 6H, 2 of (CH$_2$)$_2$**CH$_3$**), 1.25 (t, $J=7.10$, 6H, 2 of COOCH$_2$**CH$_3$**), 1.56–1.75 (m, 4H, 2 of CH$_2$**CH$_2$**CH$_3$), 2.57–2.64 (m, 2H, 2 of **H**CHCH$_2$CH$_3$), 2.80–2.88 (m, 2H, 2 of HC**H**CH$_2$CH$_3$), 4.06–4.18 (m, 4H, 2 of COO**CH$_2$**), 5.05 (s, 1H, C_4-**H**), 5.77 (s, 1H, N**H**), 7.33 (t, $J=7.58$ Hz, 1H, $C_{5'}$-**H**), 7.44 (d, $J=7.58$ Hz, 1H, $C_{4'}$-**H**), 7.57 (d, $J=7.58$ Hz, 1H, $C_{6'}$-**H**), 7.58 (s, 1H, $C_{2'}$-**H**). ^{13}C NMR (125 MHz, CDCl$_3$) δ (ppm): 13.9 (2 C, 2 of (CH$_2$)$_2$**CH$_3$**), 14.2 (2 C, 2 of COOCH$_2$**CH$_3$**), 21.9 (2 C, 2 of CH$_2$**CH$_2$**CH$_3$), 34.6 (2 C, 2 of **CH$_2$**CH$_2$CH$_3$), 39.8 (1 C, C_4), 59.9 (2 C, 2 of COO**CH$_2$**), 102.9 (2 C, C_3, and C_5), 111.7 (1 C, $C_{3'}$), 119.4 (1 C, CN), 128.5 (1 C, $C_{5'}$), 129.8 (1 C, $C_{4'}$), 131.8 (1 C, $C_{6'}$), 132.7 (1 C, $C_{2'}$), 148.8 (2 C, C_2, and C_6), 149.2 (1 C, $C_{1'}$), 166.7 (2 C, COO). ESI–MS: m/z (% abundance): 410.8 (M^+,

27), 409.8 ($[M-1]^+$, 100). Anal. (%) for $C_{24}H_{30}N_2O_4$, calcd. (found), C 70.22 (70.48), H 7.37 (7.42), N 6.82 (6.61).

5.1.2. General procedure for the synthesis of asymmetric compounds (2a-l)
A mixture of 3-cyanobenzaldehyde (0.500g, 3.813 mmol), respective alkyl acetoacetate (3.813 mmol), and respective alkyl 3-amino-crotonates (3.813 mmol) in methanol (10 mL) was added to a 50 mL round-bottomed flask. The reaction mixture was kept away from light and heated for 24h under reflux with stirring. The cooled solution was stored in the refrigerator. To obtain products (**2a-l**), the crude crystals were filtered and purified by crystallisation from methanol.

5.1.2.1. (±)-3-Isopropyl 5-methyl 4-(3-cyanophenyl)-2,6-dimethyl-1,4-dihydropyridine-3,5-dicarboxylate (2a).
Yield (0.679g, 50%) as white powder, m.p. 128–130 °C. ^{1}H NMR (400 MHz, CDCl$_3$) δ (ppm): 1.13 (d, $J=6.20$ Hz, 3H, **CH$_3$**CHCH$_3$), 1.24 (d, $J=6.20$ Hz, 3H, CH$_3$CH**CH$_3$**), 2.37 (s, 6H, C_2-**CH$_3$**, and C_6-**CH$_3$**), 3.66 (s, 3H, O**CH$_3$**), 4.95–5.01 (m, 2H, C_4-**H** and **CH**(CH$_3$)$_2$), 5.81 (s, 1H, N**H**), 7.33 (t, $J=7.59$ Hz, 1H, $C_{5'}$-**H**), 7.44 (d, $J=7.59$ Hz, 1H, $C_{4'}$-**H**), 7.56 (d, $J=7.59$ Hz, 1H, $C_{6'}$-**H**), 7.57 (s, 1H, $C_{2'}$-**H**). ESI–MS: m/z (% abundance): 354.6 (M^+, 23), 353.6 ($[M-1]^+$, 100). Anal. (%) for $C_{20}H_{22}N_2O_4$, calcd. (found), C 67.78 (67.92), H 6.26 (5.98), N 7.90 (7.92).

5.1.2.2. (±)-3-Isobutyl 5-methyl 4-(3-cyanophenyl)-2,6-dimethyl-1,4-dihydropyridine-3,5-dicarboxylate (2b).
Yield (0.853g, 61%) as white powder, m.p. 133–135 °C. ^{1}H NMR (400 MHz, CDCl$_3$) δ (ppm): 0.86 (d, $J=6.72$ Hz, 3H, **CH$_3$**CHCH$_3$), 0.89 (d, $J=6.72$ Hz, 3H, CH$_3$CH**CH$_3$**), 1.86–1.96 (m, 1H, **CH**(CH$_3$)$_2$), 2.36 (s, 3H, C_6-**CH$_3$**), 2.39 (s, 3H, C_2-**CH$_3$**), 3.68 (s, 3H, O**CH$_3$**), 3.79–3.91 (m, 2H, COO**CH$_2$**), 5.05 (s, 1H, C_4-**H**), 5.93 (s, 1H, N**H**), 7.33 (t, $J=7.76$ Hz, 1H, $C_{5'}$-**H**), 7.45 (d, $J=7.76$ Hz, 1H, $C_{4'}$-**H**), 7.53–7.63 (m, 2H, $C_{2'}$-**H** and $C_{6'}$-**H**). ^{13}C NMR (125 MHz, CDCl$_3$) δ (ppm): 19.7 (2 C, 2 of CH(**CH$_3$)$_2$**), 19.7 (2 C, C_2-**CH$_3$**, and C_6-**CH$_3$**), 27.7 (1 C, **CH**(CH$_3$)$_2$), 39.5 (1 C, C_4), 51.1 (1 C, O**CH$_3$**), 70.4 (1 C, COO**CH$_2$**), 103.2 (1 C, C_5), 103.3 (1 C, C_3), 111.9 (1 C, $C_{3'}$), 119.4 (1 C, CN), 128.6 (1 C, $C_{5'}$), 129.9 (1 C, $C_{4'}$), 131.6 (1 C, $C_{6'}$), 132.6 (1 C, $C_{2'}$), 144.6 (1 C, C_6), 144.7 (1 C, C_2), 148.9 (1 C, $C_{1'}$), 167.1 (1 C, C_3-**COO**), 167.6 (1 C, C_5-**COO**). ESI–MS: m/z (% abundance): 368.6 (M^+, 22), 367.6 ($[M-1]^+$, 100). Anal. (%) for $C_{21}H_{24}N_2O_4$, calcd. (found), C 68.46 (68.64), H 6.57 (6.39), N 7.60 (7.55).

5.1.2.3. (±)-3-Tert-butyl 5-Methyl 4-(3-cyanophenyl)-2,6-dimethyl-1,4-dihydropyridine-3,5-dicarboxylate (2c).
Yield (0.579g, 41%) as white powder, m.p. 157–159 °C. ^{1}H NMR (400 MHz, CDCl$_3$) δ (ppm): 1.32 (s, 9H, C(**CH$_3$)$_3$**), 2.25 (s, 3H, C_6-**CH$_3$**), 2.26 (s, 3H, C_2-**CH$_3$**), 3.57 (s, 3H, O**CH$_3$**), 4.88 (s, 1H, C_4-**H**), 5.59 (s, 1H, N**H**), 7.24 (t, $J=7.67$ Hz, 1H, $C_{5'}$-**H**), 7.35 (d, $J=7.67$ Hz, 1H, $C_{4'}$-**H**), 7.47 (d, $J=7.67$ Hz, 1H, $C_{6'}$-**H**), 7.48 (s, 1H, $C_{2'}$-**H**). ESI–MS: m/z (% abundance): 368.7 (M^+, 25), 367.7 ($[M-1]^+$, 100). Anal. (%) for $C_{21}H_{24}N_2O_4$, calcd. (found), C 68.46 (68.23), H 6.57 (6.87), N 7.60 (7.21).

5.1.2.4. (±)-3-(2-Methoxyethyl) 5-methyl 4-(3-cyanophenyl)-2,6-dimethyl-1,4-dihydropyridine-3,5-dicarboxylate (2d).
Yield (1.045g, 74%) as white powder, m.p. 127–128 °C. ^{1}H NMR (400 MHz, CDCl$_3$) δ (ppm): 2.37 (s, 3H, C_6-**CH$_3$**), 2.38 (s, 3H, C_2-**CH$_3$**), 3.39 (s, 3H, CH$_2$O**CH$_3$**), 3.51–3.62 (m, 2H, **CH$_2$**OCH$_3$), 3.66 (s, 3H, COO**CH$_3$**), 4.14–4.19 (m, 1H, **H**CHCH$_2$OCH$_3$), 4.23–4.29 (m, 1H, HC**H**CH$_2$OCH$_3$),

5.05 (s, 1H, C$_4$-**H**), 5.90 (s, 1H, N**H**), 7.33 (t, $J = 7.56$ Hz, 1H, C$_{5'}$-**H**), 7.45 (d, $J = 7.56$ Hz, 1H, C$_{4'}$-**H**), 7.58 (d, $J = 7.56$ Hz, 1H, C$_{6'}$-**H**), 7.59 (s, 1H, C$_{2'}$-**H**). ESI–MS: *m/z* (% abundance): 370.6 (M$^+$, 22), 369.6 ([M– 1]$^+$, 100). Anal. (%) for C$_{20}$H$_{22}$N$_2$O$_5$, calcd. (found), C 64.85 (64.86), H 5.99 (6.11), N 7.56 (7.27).

5.1.2.5. (±)-3-Benzyl 5-methyl 4-(3-cyanophenyl)-2,6-dimethyl-1,4-dihydropyridine-3,5-dicarboxylate (2e).
Yield (1.211g, 79%) as white powder, m.p. 129–131 °C. ^{1}H NMR (400 MHz, CDCl$_3$) δ (ppm): 2.36 (s, 3H, C$_6$-**CH$_3$**), 2.38 (s, 3H, C$_2$-**CH$_3$**), 3.65 (s, 3H, O**CH$_3$**), 5.03 (d, $J_{gem} = 12.13$ Hz, 1H, **H**CHC$_6$H$_5$), 5.05 (s, 1H, C$_4$-**H**), 5.17 (d, $J_{gem} = 12.13$ Hz, 1H, HC**H**C$_6$H$_5$), 6.10 (s, 1H, N**H**), 7.24–7.56 (m, 9H, **C$_6$H$_5$**, C$_{2'}$-**H**, C$_{4'}$-**H**, C$_{5'}$-**H** and C$_{6'}$-**H**). ESI–MS: *m/z* (% abundance): 402.6 (M$^+$, 27), 401.6 ([M– 1]$^+$, 100). Anal. (%) for C$_{24}$H$_{22}$N$_2$O$_4$, calcd. (found), C 71.63 (71.91), H 5.51 (5.80), N 6.96 (6.67).

5.1.2.6. (±)-3-Ethyl 5-methyl 4-(3-cyanophenyl)-6-methyl-2-propyl-1,4-dihydropyridine-3,5-dicarboxylate (2f).
Yield (0.223g, 16%) as white powder, m.p. 121–122 °C. ^{1}H NMR (400 MHz, CDCl$_3$) δ (ppm): 1.02 (t, $J = 7.16$, 3H, (CH$_2$)$_2$**CH$_3$**), 1.25 (t, $J = 6.96$, 3H, COOCH$_2$**CH$_3$**), 1.59–1.75 (m, 2H, CH$_2$**CH$_2$**CH$_3$), 2.38 (s, 3H, C$_6$-**CH$_3$**), 2.64–2.80 (m, 2H, **CH$_2$**CH$_2$CH$_3$), 3.67 (s, 3H, COO**CH$_3$**), 4.06–4.18 (m, 2H, COO**CH$_2$**), 5.05 (s, 1H, C$_4$-**H**), 5.78 (s, 1H, N**H**), 7.33 (t, $J = 7.53$ Hz, 1H, C$_{5'}$-**H**), 7.45 (d, $J = 7.53$ Hz, 1H, C$_{4'}$-**H**), 7.56 (d, $J = 7.53$ Hz, 1H, C$_{6'}$-**H**), 7.57 (s, 1H, C$_{2'}$-**H**). ESI–MS: *m/z* (% abundance): 368.7 (M$^+$, 25), 367.7 ([M– 1]$^+$, 100). Anal. (%) for C$_{21}$H$_{24}$N$_2$O$_4$, calcd. (found), C 68.46 (68.50), H 6.57 (6.39), N 7.60 (7.33).

5.1.2.7. (±)-3-Ethyl 5-methyl 4-(3-cyanophenyl)-2,6-dimethyl-1,4-dihydropyridine-3,5-dicarboxylate (2g).
Yield (0.557g, 43%) as white powder, m.p. 151–153 °C. ^{1}H NMR (400 MHz, CDCl$_3$) δ (ppm): 1.24 (t, $J = 7.10$ Hz, 3H, CH$_2$**CH$_3$**), 2.37 (s, 6H, C$_2$-**CH$_3$** and C$_6$-**CH$_3$**), 3.67 (s, 3H, COO**CH$_3$**), 4.07–4.16 (m, 2H, COO**CH$_2$**), 5.03 (s, 1H, C$_4$-**H**), 5.85 (s, 1H, N**H**), 7.33 (t, $J = 7.73$ Hz, 1H, C$_{5'}$-**H**), 7.45 (d, $J = 7.73$ Hz, 1H, C$_{4'}$-**H**), 7.56 (d, $J = 7.73$ Hz, 1H, C$_{6'}$-**H**), 7.57 (s, 1H, C$_{2'}$-**H**). ESI–MS: *m/z* (% abundance): 340.5 (M$^+$, 19), 339.5 ([M– 1]$^+$, 100). Anal. (%) for C$_{19}$H$_{20}$N$_2$O$_4$, calcd. (found), C 67.05 (66.81), H 5.92 (6.15), N 8.23 (8.04).

5.1.2.8. (±)-3-Ethyl 5-isopropyl 4-(3-cyanophenyl)-2,6-dimethyl-1,4-dihydropyridine-3,5-dicarboxylate (2h).
Yield (0.361g, 26%) as yellow powder, m.p. 136–138 °C. ^{1}H NMR (400 MHz, CDCl$_3$) δ (ppm): 1.13 (d, $J = 6.12$ Hz, 3H, **CH$_3$**CHCH$_3$), 1.24 (t, $J = 7.04$ Hz, 3H, CH$_2$**CH$_3$**), 1.27 (d, $J = 6.12$ Hz, 3H, CH$_3$CH**CH$_3$**), 2.37 (s, 6H, C$_2$-**CH$_3$**, and C$_6$-**CH$_3$**), 4.05–4.18 (m, 2H, **CH$_2$**CH$_3$), 4.93–5.03 (m, 2H, **CH**(CH$_3$)$_2$ and C$_4$-**H**), 5.77 (s, 1H, N**H**), 7.32 (t, $J = 7.56$ Hz, 1H, C$_{5'}$-**H**), 7.44 (d, $J = 7.56$ Hz, 1H, C$_{4'}$-**H**), 7.57 (d, $J = 7.56$ Hz, 1H, C$_{6'}$-**H**), 7.58 (s, 1H, C$_{2'}$-**H**). ESI–MS: *m/z* (% abundance): 368.7 (M$^+$, 23), 367.7 ([M– 1]$^+$, 100). Anal. (%) for C$_{21}$H$_{24}$N$_2$O$_4$, calcd. (found), C 68.46 (68.57), H 6.57 (6.33), N 7.60 (7.45).

5.1.2.9. (±)-3-Ethyl 5-isobutyl 4-(3-cyanophenyl)-2,6-dimethyl-1,4-dihydropyridine-3,5-dicarboxylate (2i).
Yield (0.299g, 21%) as yellow powder, m.p. 120–121 °C. ^{1}H NMR (400 MHz, CDCl$_3$) δ (ppm): 0.87 (d, $J = 6.72$ Hz, 3H, **CH$_3$**CHCH$_3$), 0.90 (d, $J = 6.72$ Hz, 3H, CH$_3$CH**CH$_3$**), 1.26 (t, $J = 7.16$ Hz, 3H, CH$_2$**CH$_3$**), 1.86–1.96 (m, 1H, **CH**(CH$_3$)$_2$, 2.37 (s, 3H, C$_2$-**CH$_3$**), 2.40 (s, 3H, C$_6$-**CH$_3$**), 3.80–3.90 (m, 2H, COO**CH$_2$**CH$_3$), 4.07–4.17 (m, 2H, COO**CH$_2$**CH), 5.06 (s, 1H, C$_4$-**H**), 5.85 (s, 1H, N**H**), 7.33 (t, $J = 7.79$ Hz, 1H, C$_{5'}$-**H**), 7.45 (d, $J = 7.79$ Hz, 1H, C$_{4'}$-**H**), 7.58 (d, $J = 7.79$ Hz, 1H, C$_{6'}$-**H**), 7.59 (s, 1H, C$_{2'}$-**H**). ESI–MS: *m/z* (% abundance): 382.7 (M$^+$, 25), 381.7 ([M– 1]$^+$, 100).

Anal. (%) for C$_{22}$H$_{26}$N$_2$O$_4$, calcd. (found), C 69.09 (69.18), H 6.85 (7.00), N 7.32 (7.10).

5.1.2.10. (±)-3-Tert-butyl 5-ethyl 4-(3-cyanophenyl)-2,6-dimethyl-1,4-dihydropyridine-3,5-dicarboxylate (2j).
Yield (0.623g, 43%) as yellow powder, m.p. 152–153 °C. ^{1}H NMR (400 MHz, CDCl$_3$) δ (ppm): 1.24 (t, $J = 7.10$ Hz, 3H, CH$_2$**CH$_3$**), 1.41 (s, 9H, C(**CH$_3$**)$_3$), 2.34 (s, 3H, C$_6$-**CH$_3$**), 2.36 (s, 3H, C$_2$-**CH$_3$**), 4.07–4.16 (m, 2H, COO**CH$_2$**), 4.98 (s, 1H, C$_4$-**H**), 5.65 (s, 1H, N**H**), 7.33 (t, $J = 7.56$ Hz, 1H, C$_{5'}$-**H**), 7.45 (d, $J = 7.56$ Hz, 1H, C$_{4'}$-**H**), 7.57 (d, $J = 7.56$ Hz, 1H, C$_{6'}$-**H**), 7.58 (s, 1H, C$_{2'}$-**H**). ^{13}C NMR (125 MHz, CDCl$_3$) δ (ppm): 14.2 (1 C, CH$_2$**CH$_3$**), 19.6 (1 C, C$_6$-**CH$_3$**), 19.7 (1 C, C$_2$-**CH$_3$**), 28.2 (3 C, C(**CH$_3$**)$_3$), 40.0 (1 C, C$_4$), 59.9 (1 C, COO**CH$_2$**), 80.2 (1 C, **C**(CH$_3$)$_3$), 103.0 (1 C, C$_5$), 104.8 (1 C, C$_3$), 111.7 (1 C, C$_{3'}$), 119.4 (1 C, CN), 128.4 (1 C, C$_{5'}$), 129.7 (1 C, C$_{4'}$), 131.9 (1 C, C$_{6'}$), 132.8 (1 C, C$_{2'}$), 143.4 (1 C, C$_6$), 144.5 (1 C, C$_2$), 149.2 (1 C, C$_{1'}$), 166.4 (1 C, C$_3$-**COO**), 167.2 (1 C, C$_5$-**COO**). ESI–MS: *m/z* (% abundance): 382.6 (M$^+$, 26), 381.6 ([M– 1]$^+$, 100). Anal. (%) for C$_{22}$H$_{26}$N$_2$O$_4$, calcd. (found), C 69.09 (68.96), H 6.85 (7.15), N 7.32 (7.02).

5.1.2.11. (±)-3-Ethyl 5-(2-methoxyethyl) 4-(3-cyanophenyl)-2,6-dimethyl-1,4-dihydropyridine-3,5-dicarboxylate (2k).
Yield (0.629g, 43%) as yellowish white powder, m.p. 133–134 °C. ^{1}H NMR (400 MHz, CDCl$_3$) δ (ppm): 1.23 (t, $J = 7.10$ Hz, 3H, CH$_2$**CH$_3$**), 2.37 (s, 3H, C$_2$-**CH$_3$**), 2.38 (s, 3H, C$_6$-**CH$_3$**), 3.39 (s, 3H, O**CH$_3$**), 3.52–3.62 (m, 2H, **CH$_2$**OCH$_3$), 4.06–4.27 (m, 4H, **CH$_2$**CH$_3$ and COO**CH$_2$**), 5.05 (s, 1H, C$_4$-**H**), 5.84 (s, 1H, N**H**), 7.33 (t, $J = 7.66$ Hz, 1H, C$_{5'}$-**H**), 7.45 (d, $J = 7.66$ Hz, 1H, C$_{4'}$-**H**), 7.59 (d, $J = 7.66$ Hz, 1H, C$_{6'}$-**H**), 7.61 (s, 1H, C$_{2'}$-**H**). ESI–MS: *m/z* (% abundance): 384.8 (M$^+$, 20), 383.8 ([M– 1]$^+$, 100). Anal. (%) for C$_{21}$H$_{24}$N$_2$O$_5$, calcd. (found), C 65.61 (65.35), H 6.29 (6.09), N 7.29 (6.97).

5.1.2.12. (±)-3- Benzyl 5-ethyl 4-(3-cyanophenyl)-2,6-dimethyl-1,4-dihydropyridine-3,5-dicarboxylate (2l).
Yield (1.208g, 76%) as off-white powder, m.p. 115–117 °C. ^{1}H NMR (400 MHz, CDCl$_3$) δ (ppm): 1.22 (t, $J = 7.12$ Hz, 3H, CH$_2$**CH$_3$**), 2.37 (s, 3H, C$_6$-**CH$_3$**), 2.39 (s, 3H, C$_2$-**CH$_3$**), 4.04–4.16 (m, 2H, **CH$_2$**CH$_3$), 5.04 (d, $J_{gem} = 12.40$ Hz, 1H, **H**CHC$_6$H$_5$), 5.05 (s, 1H, C$_4$-**H**), 5.16 (d, $J_{gem} = 12.40$ Hz, 1H, HC**H**C$_6$H$_5$), 5.80 (s, 1H, N**H**), 7.22–7.52 (m, 9H, **C$_6$H$_5$**, C$_{2'}$-**H**, C$_{4'}$-**H**, C$_{5'}$-**H** and C$_{6'}$-**H**). ^{13}C NMR (125 MHz, CDCl$_3$) δ (ppm): 14.2 (1 C, CH$_2$**CH$_3$**), 19.6 ((1 C, C$_6$-**CH$_3$**), 19.7 (1 C, C$_2$-**CH$_3$**), 39.7 (1 C, C$_4$), 59.9 (1 C, **CH$_2$**CH$_3$), 65.9 (1 C, **CH$_2$**C$_6$H$_5$), 102.9 (1 C, C$_5$), 103.5 (1 C, C$_3$), 111.7 (1 C, C$_{3'}$), 119.3 (1 C, CN), 128.0 (2 C, C$_2$ and C$_6$ of C$_6$H$_5$), 128.5 (3 C, C$_3$, C$_4$ and C$_5$ of C$_6$H$_5$), 128.5 (1 C, C$_{5'}$), 129.8 (1 C, C$_{4'}$), 131.9 (1 C, C$_{6'}$), 132.9 (1 C, C$_{2'}$), 136.1 (1 C, C$_1$ of C$_6$H$_5$), 144.3 (1 C, C$_6$), 145.2 (1 C, C$_6$), 149.0 (1 C, C$_{1'}$), 166.8 (1 C, C$_5$-**COO**), 167.0 (1 C, C$_3$-**COO**). ESI–MS: *m/z* (% abundance): 416.8 (M$^+$, 26), 415.8 ([M– 1]$^+$, 100). Anal. (%) for C$_{25}$H$_{24}$N$_2$O$_4$, calcd. (found), C 72.10 (71.99), H 5.81 (5.96), N 6.73 (6.54).

5.2. Pharmacological evaluation of target compounds

5.2.1. Anticancer activity

5.2.1.1. In vitro *single dose (10 μM) anticancer screening on NCI 60 cancer cell lines.*
All 60 cancer cell lines were cultured in RPMI 1640 medium. Cells were inoculated into 96 well microtiter plates then incubated in 5% CO$_2$, 95% air, and 100% relative humidity for 24h at 37 °C, before the tested compound was added. After 24h, trichloroacetic acid (TCA) was used to fix two plates of each cell line (one as a test and the other as a control) *in situ* to reflect a measurement of cell population for each cell line at time zero of compound addition (Tz). Prior to usage, the tested chemical was

solubilised in 400-fold the intended final maximum test concentration in DMSO and stored frozen. The needed final compound concentration was achieved by adding aliquots of 100 μL of this chemical's solution to appropriate microtiter wells already holding 100 μL of medium. Following the addition of the chemical, the two plates were incubated for an additional 48h at 37 °C, 5% CO_2, 95% air, and 100% relative humidity. The test was ended by the addition of cold TCA for adhering cells. The cells were fixed *in situ* by gently adding 50 μL of cold 50% (w/v) TCA (final concentration, 10% TCA) and incubating at 4 °C for 60 min. The supernatant was discarded, and the plates were rinsed and air dried five times with tap water. SRB solution (100 μL) containing 0.4% (w/v) sulforhodamine in 1% acetic acid was added to each well, and plates were incubated at room temperature for 10 min. The bound dye was then solubilised with 10 mM trizma base, and the absorbance was measured at 515 nm using an automated plate reader.[57,58]

5.2.1.2. In vitro *cytotoxicity of target compounds, 1g, 2e, and 2l in human HCT-116 and HCT-116/ADR cells and their potentiation of DOX cytotoxicity in drug-resistant HCT-116/ADR cell.* We investigated the reversal DOX effect of the three most active compounds, **1g**, **2e**, and **2l**, and assessed the IC_{50} of DOX and RF, which was measured by dividing the IC_{50} (DOX) values without P-gp modulators by IC_{50} (DOX) values with P-gp modulators as previously described.[77,78]

5.2.1.3. Mechanistic insight of 1g, 2e, and 2l induced cytotoxicity.
EGFR, HER-2, and BTK inhibitory activity of the potent antitumor compounds **1g**, **2e**, and **2l** were studied, and results were displayed as IC_{50} (nM) and % potency, and they are compared to erlotinib as a reference drug as previously described.[15]

5.2.1.4. Annexin V–FITC apoptosis assay. PS externalisation was identified using the apoptosis detection kit (Annexin V-FITC/PI) (BD Biosciences) in accordance with the manufacturer's guidelines.[79]

5.2.1.5. In vitro *cell cycle analysis.* HCT-116 cells were treated for 24h with the IC_{50} concentrations of DHPs **1g**, **2e**, and **2l**, then washed three times with cold phosphate buffered saline. The cells were centrifuged, frozen in cold 75% ethanol, washed in phosphate buffered saline, resuspended with 100 mg/mL RNase, then stained with 40 mg/mL PI, and analysed with a FACS Calibur (Becton Dickinson, BD, Franklin Lakes, NJ). The cell cycle distributions were determined using Becton Dickinson's CellQuest software version 5.1.[80]

5.2.2. Antimicrobial activity
5.2.2.1. In vitro *antibacterial and antifungal evaluation.* By the agar well diffusion method, all of the synthesised compounds were individually evaluated against six pathogen strains; two gram-positive bacteria (*S. aureus* and *B. subtilis*), two gram-negative bacteria (*E. coli* and *P. aeruginosa*), and two fungi (*C. albicans* and *A. flavus*). To make a 1 mg/mL solution, each chemical was dissolved separately and aseptically in DMSO. Whatman filter paper discs of a standard size (5 mm diameter) were manufactured, cut, and sterilised in an autoclave. The paper discs were soaked in the compound solution to the necessary concentration before being inserted aseptically on petri plates containing nutrient agar media (20g agar, 3g beef extract, and 5g peptone) inoculated with the pathogen under study. After 24h of incubation at

36 °C, the inhibition zones were measured in millimetres. Standard antibacterial and antifungal compounds, ciprofloxacin and clotrimazole, were employed in the same operation and under the same settings. As a control, DMSO solvent was employed. Three times each treatment was carried out.[51,67]

5.2.2.2. Determination of minimum inhibitory concentration (MIC).
The MIC of selected compounds **1f**, **1g**, **2a**, **2g**, **2j, and 2k** were determined by using the two-fold microbroth dilution method. The selected compounds' solutions in different concentrations of 64, 32, 16, 8, 4, 2, 1, and 0.5 μg/mL were aseptically prepared using DMSO as a solvent and put in different wells. The broth containing the tested pathogen suspension at 106 CFU/mL was added evenly to each well. The sealed plates were incubated at 36 °C for 24h. Ciprofloxacin and clotrimazole were used as standard antibacterial and antifungal agents, respectively, using the same procedure under the same conditions. Positive control of wells with DMSO and inoculated media and negative control of wells with DMSO and uninoculated media were run parallel to each tested compound experiment. Each experiment was performed in triplicate. MIC was determined as the lowest concentration that had no visible turbidity.[68]

5.3. Molecular docking

For complex modelling, the RSCB Protein Data Bank was used to obtain the structure of various proteins (PDB IDs: 4MS2, 3G60, 1M17, 3RCD, and 4Z3V). The MOE suite was utilised to create target compound structures. A Tripos force field and energy minimisation were used to optimise the structure in vacuum. The partial atomic charges were calculated using the Gasteiger–Huckel method. The docking was done with the MOE package. The MOE Tools package was used to set the docking parameters. The ligand poses obtained through docking were graded and chosen based on the values of their scoring functions and poses in the binding site. Crystal structure ligand locations were used as a reference template to assess the docked molecules' correctness.[81]

ORCID

Ahmed B. M. Mehany 🔟 http://orcid.org/0000-0002-9913-5380
Amany Belal 🔟 http://orcid.org/0000-0003-1045-0163
Mohammed A. S. Abourehab 🔟 http://orcid.org/0000-0003-1348-6567
Haytham O. Tawfik 🔟 http://orcid.org/0000-0001-6455-5716

References

1. Chen S, Zhao Y, Liu S, et al. Epigenetic enzyme mutations as mediators of anti-cancer drug resistance. Drug Resistance Updates 2022;61:100821–13.

2. Gupta N, Huang TT, Horibata S, Lee JM. Cell cycle checkpoints and beyond: exploiting the ATR/CHK1/WEE1 pathway for the treatment of PARP inhibitor–resistant cancer. Pharmacol Res 2022;178:106162–12.

3. Tu SM, Guo CC, Chow DSL, Zacharias NM. Stem cell theory of cancer: implications for drug resistance and chemosensitivity in cancer care. Cancers 2022;14:1548–11.

4. Li X, Li M, Huang M, et al. The multi-molecular mechanisms of tumor-targeted drug resistance in precision medicine. Biomed Pharmacother 2022;150:113064–15.

5. Friedlaender A, Subbiah V, Russo A, et al. EGFR and HER2 exon 20 insertions in solid tumours: from biology to treatment. Nat Rev Clin Oncol 2022;19:51–69.

6. Sitthideatphaiboon P, Teerapakpinyo C, Korphaisarn K, et al. Co-occurrence CDK4/6 amplification serves as biomarkers of de novo EGFR TKI resistance in sensitizing EGFR mutation non-small cell lung cancer. Sci Rep 2022;12:13.

7. Hu L, Fan M, Shi S, et al. Dual target inhibitors based on EGFR: promising anticancer agents for the treatment of cancers. Eur J Med Chem 2017;227:1–25.

8. Jiwacharoenchai N, Saruengkhanphasit R, Niwetmarin W, et al. Discovery of potent antiproliferative agents from selected oxygen heterocycles as EGFR tyrosine kinase inhibitors from the US National Cancer Institute database by in silico screening and bioactivity evaluation. Bioorg Med Chem Lett 2022;58:128524–5.

9. Sun W, Ma Z, Yan H. Biological evaluation of 4-aryl-1,4-dihydropyridines as VEGFR-2 kinase inhibitors. Russian J Gen Chem 2016;86:2891–9.

10. Deswal N, Shrivastava A, Summon Hossain M, et al. Design, synthesis, evaluation and molecular docking studies of novel triazole linked 1,4-dihydropyridine-isatin scaffolds as potent anticancer agents. ChemistrySelect 2021;6:717–25.

11. Mansour B, Bayoumi WA, El-Sayed MA, et al. In vitro cytotoxicity and docking study of novel symmetric and asymmetric dihydropyridines and pyridines as EGFR tyrosine kinase inhibitors. Chem Biol Drug Design 2022;100:121–135.

12. Mohamed MF, Darweesh AF, Elwahy AH, Abdelhamid IA. Synthesis, characterization and antitumor activity of novel tetrapodal 1,4-dihydropyridines: p53 induction, cell cycle arrest and low damage effect on normal cells induced by genotoxic factor H2O2. RSC Adv 2016;6:40900–10.

13. Manna D, Bhuyan R, Ghosh R. Probing the mechanism of SIRT1 activation by a 1,4-dihydropyridine. J Mol Modeling 2018;24:1–12.

14. Manna D, Bhuyan R, Saikh F, et al. Novel 1,4-dihydropyridine induces apoptosis in human cancer cells through overexpression of Sirtuin1. Apoptosis 2018;23:532–53.

15. Sidhom PA, El-Bastawissy E, Salama AA, El-Moselhy TF. Revisiting ageless antiques; synthesis, biological evaluation, docking simulation and mechanistic insights of 1,4-Dihydropyridines as anticancer agents. Bioorg Chem 2021;114:105054.

16. Cancer multidrug resistance. Nat Biotechnol 2000;18:18–20.

17. Mansoori B, Mohammadi A, Davudian S, et al. The different mechanisms of cancer drug resistance: a brief review. Adv Pharm Bull 2017;7:339–48.

18. Choi YH, Yu A-M. ABC transporters in multidrug resistance and pharmacokinetics, and strategies for drug development. Curr Pharm Design 2014;20:793–807.

19. Leslie EM, Deeley RG, Cole SP. Multidrug resistance proteins: role of P-glycoprotein, MRP1, MRP2, and BCRP (ABCG2) in tissue defense. Toxicol Appl Pharmacol 2005;204:216–37.

20. Maki N, Hafkemeyer P, Dey S. Allosteric modulation of human P-glycoprotein: inhibition of transport by preventing substrate translocation and dissociation. J Biol Chem 2003;278:18132–9.

21. Zarrin A, Mehdipour AR, Miri R. Dihydropyridines and multidrug resistance: previous attempts, present state, and future trends. Chem Biol Drug Design 2010;76:369–81.

22. Ojima I, Bounaud PY, Oderda CF. Recent strategies for the treatment of multi-drug resistance in cancer cells. Exp Opin Ther Patents 1998;8:1587–98.

23. Sirisha K, Shekhar MC, Umasankar K, et al. Molecular docking studies and in vitro screening of new dihydropyridine derivatives as human MRP1 inhibitors. Bioorg Med Chem 2011;19:3249–54.

24. Sirisha K, Achaiah G, Reddy VM. Facile synthesis and antibacterial, antitubercular, and anticancer activities of novel 1,4-dihydropyridines. Arch Pharm 2010;343:342–52.

25. Vijesh A, Isloor AM, Peethambar S, et al. Hantzsch reaction: synthesis and characterization of some new 1,4-dihydropyridine derivatives as potent antimicrobial and antioxidant agents. Eur J Med Chem 2011;46:5591–7.

26. Perumal M, Sengodu P, Venkatesan S, et al. Polybenzimidazole-triphenylphosphene-catalyzed one-pot synthesis and evaluation of dihydropyridine derivative as antibiotics and antifungals. ChemistrySelect 2017;2:7489–96.

27. Mahinpour R, Moradi L, Zahraei Z, Pahlevanzadeh N. New synthetic method for the synthesis of 1,4-dihydropyridine using aminated multiwalled carbon nanotubes as high efficient catalyst and investigation of their antimicrobial properties. J Saudi Chem Soc 2018;22:876–85.

28. Abu-Melha H. Synthesis, antibacterial and antifungal evaluation of novel 1,4-dihydropyridine derivatives. Spectrochim Acta A Mol Biomol Spectrosc 2013;113:115–22.

29. Bucaneve G, Micozzi A, Menichetti F, et al. Levofloxacin to prevent bacterial infection in patients with cancer and neutropenia. New England J Med 2005;353:977–87.

30. Azevedo MM, Pina-Vaz C, Baltazar F. Microbes and cancer: friends or faux? Int J Mol Sci 2020;21:3115–23.

31. Rolston KV. Challenges in the treatment of infections caused by gram-positive and gram-negative bacteria in patients with cancer and neutropenia. Clin Infect Dis 2005;40:S246–S252.

32. Khatun S, Appidi T, Rengan AK. The role played by bacterial infections in the onset and metastasis of cancer. Curr Res Microb Sci 2021;2:100078–19.

33. Elsland D, Neefjes J. Bacterial infections and cancer. EMBO Rep 2018;19:e46632.

34. Azap A, Bozkurt GY, Yüksel MK, et al. Secondary infections in cancer patients with febrile neutropenia. Turk J Hematol 2012;29:254–8.

35. Fleming FF, Yao L, Ravikumar P, et al. Nitrile-containing pharmaceuticals: efficacious roles of the nitrile pharmacophore. J Med Chem 2010;53:7902–17.

36. Wang X, Wang Y, Li X, et al. Nitrile-containing pharmaceuticals: target, mechanism of action, and their SAR studies. RSC Med Chem 2021;12:1650–71.

37. Berteotti A, Vacondio F, Lodola A, et al. Predicting the reactivity of nitrile-carrying compounds with cysteine: a combined computational and experimental study. ACS Med Chem Lett 2014;5:501–5.

38. Fares S, Selim KB, Goda FE, et al. Design, synthesis, and analysis of antiproliferative and apoptosis-inducing activities of nitrile derivatives containing a benzofuran scaffold: EGFR inhibition assay and molecular modelling study. J Enzyme Inhibit Med Chem 2021;36:1488–99.

39. Nasser AA, Eissa IH, Oun MR, et al. Discovery of new pyrimidine-5-carbonitrile derivatives as anticancer agents targeting EGFR WT and EGFR T790M. Organic Biomol Chem 2020;18:7608–34.

40. Belal A, Abdel Gawad NM, Mehany ABM, et al. Design, synthesis and molecular docking of new fused 1H-pyrroles, pyrrolo[3,2-d]pyrimidines and pyrrolo[3,2-e][1, 4]diazepine derivatives as potent EGFR/CDK2 inhibitors. J Enzyme Inhibit Med Chem 2022;37:1884–902.

41. Ahmed NM, Youns MM, Soltan MK, Said AM. Design, synthesis, molecular modeling and antitumor evaluation of novel indolyl-pyrimidine derivatives with EGFR inhibitory activity. Molecules 2021;26:1838.

42. Suresh S, Das S, Waidha K, et al. Multi-component approach for synthesis of quinolinyl-1, 4-dihydropyridines, evaluation of cytotoxicity against MCF7 and molecular docking studies. ChemistrySelect 2020;5:10501–10.

43. Wang B, Zhao B, Chen ZS, et al. Exploration of 1, 2, 3-triazole-pyrimidine hybrids as potent reversal agents against ABCB1-mediated multidrug resistance. Eur J Med Chem 2018;143:1535–42.

44. Zhang H, Xu H, Ashby CR, Jr, et al. Chemical molecular-based approach to overcome multidrug resistance in cancer by targeting P-glycoprotein (P-gp). Med Res Rev 2021;41:525–55.

45. Rashid M, Malik MY, Singh SK, et al. Bioavailability enhancement of poorly soluble drugs: the holy grail in pharma industry. Curr Pharm Design 2019;25:987–1020.

46. Wang B, Ma LY, Wang JQ, et al. Discovery of 5-cyano-6-phenylpyrimidin derivatives containing an acylurea moiety as orally bioavailable reversal agents against P-glycoprotein-mediated mutidrug resistance. J Med Chem 2018;61:5988–6001.

47. Ranjbar S, Edraki N, Firuzi O, et al. 5-Oxo-hexahydroquinoline: an attractive scaffold with diverse biological activities. Mol Div 2019;23:471–508.

48. Nkosi SM, Anand K, Anandakumar S, et al. Design, synthesis, anticancer, antimicrobial activities and molecular docking studies of novel quinoline bearing dihydropyridines. J Photochem Photobiol B Biol 2016;165:266–76.

49. Reddy GM, Camilo A. Jr, Biologically active dihydropyridines: an efficient green synthesis, antimicrobial properties, machine aided results and SARs. Sustain Chem Pharm 2020;17:100303–8.

50. Altalbawy FM. Synthesis and antimicrobial evaluation of some novel bis-α, β-unsaturated ketones, nicotinonitrile, 1, 2-dihydropyridine-3-carbonitrile, fused thieno [2, 3-b] pyridine and pyrazolo [3, 4-b] pyridine derivatives. Int J Mol Sci 2013;14:2967–79.

51. Refat HM, Fadda A. Synthesis and antimicrobial activity of some novel hydrazide, benzochromenone, dihydropyridine, pyrrole, thiazole and thiophene derivatives. Eur J Med Chem 2013;70:419–26.

52. Ragab A, Fouad SA, Ali OAA, et al. Sulfaguanidine hybrid with some new pyridine-2-one derivatives: design, synthesis, and antimicrobial activity against multidrug-resistant bacteria as dual DNA gyrase and DHFR inhibitors. Antibiotics 2021;10:162–31.

53. Murphy ST, Case HL, Ellsworth E, et al. The synthesis and biological evaluation of novel series of nitrile-containing fluoroquinolones as antibacterial agents. Bioorg Med Chem Lett 2007;17:2150–5.

54. Hantzsch A. Ueber die synthese pyridinartiger verbindungen aus acetessigäther und aldehydammoniak. Justus Liebigs Annalen Chem 1882;215:1–82.

55. Iwanami M, Shibanuma T, Fujimoto M, et al. Synthesis of new water-soluble dihydropyridine vasodilators. Chem Pharm Bull 1979;27:1426–40.

56. Miri R, Javidnia K, Kebriaie-Zadeh A, et al. Synthesis and evaluation of pharmacological activities of 3,5-dialkyl 1,4-dihydro-2,6-dimethyl-4-nitroimidazole-3,5-pyridine dicarboxylates. Arch Der Pharm 2003;336:422–8.

57. Takimoto CH. Anticancer drug development at the US National Cancer Institute. Cancer Chemother Pharmacol 2003;52:29–33.

58. Monga M, Sausville EA. Developmental therapeutics program at the NCI: molecular target and drug discovery process. Leukemia 2002;16:520–6.

59. Hohla F, Buchholz S, Schally AV, et al. Targeted cytotoxic somatostatin analog AN-162 inhibits growth of human colon carcinomas and increases sensitivity of doxorubicin resistant murine leukemia cells. Cancer Lett 2010;294:35–42.

60. Hammoud MM, Nageeb AS, Morsi M, et al. Design, synthesis, biological evaluation, and SAR studies of novel cyclopenta-quinoline derivatives as DNA intercalators, topoisomerase II inhibitors, and apoptotic inducers. New J Chem 2022;46:11422–36.

61. Ren YJ, Wang ZC, Zhang X, et al. EGFR/HER-2 inhibitors: synthesis, biological evaluation and 3D-QSAR analysis of dihydropyridine-containing thiazolinone derivatives. RSC Adv 2015;5:21445–54.

62. Abdel-Aziz AA-M, El-Azab AS, AlSaif NA, et al. Synthesis, potential antitumor activity, cell cycle analysis, and multitarget mechanisms of novel hydrazones incorporating a 4-methylsulfonylbenzene scaffold: a molecular docking study. J Enzyme Inhib Med Chem 2021;36:1520–38.

63. Pfeffer CM, Singh AT. Apoptosis: a target for anticancer therapy. Int J Mol Sci 2018;19:448–57.

64. Vermes I, Haanen C, Steffens-Nakken H, Reutelingsperger C. A novel assay for apoptosis flow cytometric detection of phosphatidylserine expression on early apoptotic cells using fluorescein labelled Annexin V. J Immunol Methods 1995;184:39–51.

65. Abdelrahman MA, Eldehna WM, Nocentini A, et al. Novel diamide-based benzenesulfonamides as selective carbonic anhydrase IX inhibitors endowed with antitumor activity: synthesis, biological evaluation and in silico insights. Int J Mol Sci 2019;20:2484–99.

66. Otto T, Sicinski P. Cell cycle proteins as promising targets in cancer therapy. Nat Rev Cancer 2017;17:93–115.

67. Shaaban S, Negm A, Sobh MA, Wessjohann LA. Organoselenocyanates and symmetrical diselenides redox modulators: design, synthesis and biological evaluation. Eur J Med Chem 2015;97:190–201.

68. Ahamed A, Arif IA, Mateen M, et al. Antimicrobial, anticoagulant, and cytotoxic evaluation of multidrug resistance

of new 1,4-dihydropyridine derivatives. Saudi J Biol Sci 2018; 25:1227–35.

69. Mollazadeh S, Sahebkar A, Kalalinia F, et al. Synthesis, in silico and in vitro studies of new 1,4-dihydropiridine derivatives for antitumor and P-glycoprotein inhibitory activity. Bioorg Chem 2019;91:103156–66.

70. Aziz MW, Kamal AM, Mohamed KO, Elgendy AA. Design, synthesis and assessment of new series of quinazolinone derivatives as EGFR inhibitors along with their cytotoxic evaluation against MCF7 and A549 cancer cell lines. Bioorg Med Chem Lett 2021;41:127987–97.

71. Zou M, Li J, Jin B, et al. Design, synthesis and anticancer evaluation of new 4-anilinoquinoline-3-carbonitrile derivatives as dual EGFR/HER2 inhibitors and apoptosis inducers. Bioorg Chem 2021;114:105200–10.

72. Zhang D, Gong H, Meng F. Recent advances in BTK Inhibitors for the treatment of inflammatory and auto-immune diseases. Molecules 2021;26:4907–41.

73. Ishikawa T, Seto M, Banno H, et al. Design and synthesis of novel human epidermal growth factor receptor 2 (HER2)/ epidermal growth factor receptor (EGFR) dual inhibitors bearing a pyrrolo [3,2-d] pyrimidine scaffold. J Med Chem 2011;54:8030–50.

74. Mao C, Zhou M, Uckun FM. Crystal structure of Bruton's tyrosine kinase domain suggests a novel pathway for activation and provides insights into the molecular basis of X-linked agammaglobulinemia. J Biol Chem 2001;276: 41435–43.

75. Sultan MM, Denny RA, Unwalla R, et al. Millisecond dynamics of BTK reveal kinome-wide conformational plasticity within the apo kinase domain. Sci Rep 2017;7:15604–15.

76. El-Moselhy T. Synthesis of 1,4-dihydropyridine Hantzsch esters as potential calcium channel blockers. Alexandria J Pharm Sci 2002;16:35–9.

77. Bazargan L, Fouladdel S, Shafiee A, et al. Evaluation of anti-cancer effects of newly synthesized dihydropyridine derivatives in comparison to verapamil and doxorubicin on T47D parental and resistant cell lines in vitro. Cell Biol Toxicol 2008;24:165–74.

78. Cindric M, Cipak ANA, Serly J, et al. Reversal of multidrug resistance in murine lymphoma cells by amphiphilic dihydropyridine antioxidant derivative. Anticancer Res 2010;30: 4063–94069.

79. Eldehna WM, Abo-Ashour MF, Ibrahim HS, et al. Novel [(3-indolylmethylene) hydrazono] indolin-2-ones as apoptotic anti-proliferative agents: design, synthesis and in vitro biological evaluation. J Enzyme Inhibit Med Chem 2018;33: 686–700.

80. Mohamed MF, Abdelmoniem AM, Elwahy AH, Abdelhamid IA. DNA fragmentation, cell cycle arrest, and docking study of novel bis spiro-cyclic 2-oxindole of pyrimido [4,5-b] quin-oline-4, 6-dione derivatives against breast carcinoma. Curr Cancer Drug Targets 2018;18:372–81.

81. Vilar S, Cozza G, Moro S. Medicinal chemistry and the molecular operating environment (MOE): application of QSAR and molecular docking to drug discovery. Curr Top Med Chem 2008;8:1555–72.